GL-TR-90-0116

AD-A223 486

Siting Survey and Configuration Optimization
of a New Regional Array in the Federal
Republic of Germany

H-P. Harjes

Ruhr-University Bochum
D-4630 Bochum
FEDERAL REPUBLIC OF GERMANY

15 March 1990

Final Report
15 December 1988–15 December 1989

DTIC
JUL 03 1990
D

90 07 3 169

This technical report has been reviewed and is approved for
publication.

<table>
<tr><td>JAMES F. LEWKOWICZ</td><td>JAMES F. LEWKOWICZ</td></tr>
<tr><td>Contract Manager</td><td>Branch Chief</td></tr>
<tr><td>Solid Earth Geophysics Branch</td><td>Solid Earth Geophysics Branch</td></tr>
<tr><td>Earth Sciences Division</td><td>Earth Sciences Division</td></tr>
</table>

FOR THE COMMANDER
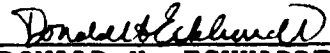
DONALD H. ECKHARDT, Director
Earth Sciences Division

REPORT DOCUMENTATION PAGE

REPORT SECURITY CLASSIFICATION Unclassified		1b RESTRICTIVE MARKINGS			
2a SECURITY CLASSIFICATION AUTHORITY		3 DISTRIBUTION/AVAILABILITY OF REPORT Approved for public release; Distribution unlimited			
2b DECLASSIFICATION DOWNGRADING SCHEDULE					
4 PERFORMING ORGANIZATION REPORT NUMBER(S) RUB-90-100		5 MONITORING ORGANIZATION REPORT NUMBER(S) GL-TR-90-0116			
6a NAME OF PERFORMING ORGANIZATION Ruhr University Bochum	6b OFFICE SYMBOL (If applicable)	7a NAME OF MONITORING ORGANIZATION Geophysics Laboratory			
6c ADDRESS (City, State, and ZIP Code) D-4630 Bochum FEDERAL REPUBLIC OF GERMANY		7b ADDRESS (City, State, and ZIP Code) Hanscom AFB Massachusetts 01731-5000			
8a NAME OF FUNDING SPONSORING ORGANIZATION DARPA	8b OFFICE SYMBOL (If applicable) NMRO	9 PROCUREMENT INSTRUMENT IDENTIFICATION NUMBER F49620-88-C-0045			
8c ADDRESS (City State, and ZIP Code) 1400 Wilson Blvd Arlington, VA 22209		10 SOURCE OF FUNDING NUMBERS			
		PROGRAM ELEMENT NO 62714E	PROJECT NO 8A10	TASK NO DA	WORK UNIT ACCESSION NO AF

11 TITLE (Include Security Classification)
Siting Survey and Configuration Optimization of a New Regional Array in the Federal Republic of Germany

12 PERSONAL AUTHOR(S)
H.-P. Harjes

13a TYPE OF REPORT FINAL	13b TIME COVERED FROM 12/15/88 to 12/15/89	14 DATE OF REPORT (Year, Month, Day) 1990 March 15	15 PAGE COUNT 74

16 SUPPLEMENTARY NOTATION

17 COSATI CODES			18 SUBJECT TERMS (Continue on reverse if necessary and identify by block number)
FIELD	GROUP	SUB GROUP	Seismic Nuclear Test Detection
			Noise
			Arrays

19 ABSTRACT (Continue on reverse if necessary and identify by block number)
This project is involved performing a siting survey for an advanced seismic array in the Federal Republic of Germany which could be used in a multi-array network jointly with arrays in Scandinavia to detect and identify seismic events especially at regional distances. In order to asses the eventual capabilities of a new high-frequency array in the FRG, it was necessary not only to conduct a noise survey but also to determine signal coherence in an area corresponding to the array aperture. After an extensive field survey, the Bavarian Forest (BF) area at the southeastern border of the FRG to Austria and Czechoslovakia was chosen as a target region to install a NORESS type array. The BF-area - as part of the Bohemian Massif - represents the largest outcropping crystalline complex in Central Europe. Detailed noise measurements show average values for the power spectrum slight **(OVER)**

20 DISTRIBUTION/AVAILABILITY OF ABSTRACT ☐ UNCLASSIFIED/UNLIMITED ☐ SAME AS RPT ☐ DTIC USERS	21 ABSTRACT SECURITY CLASSIFICATION Unclassified	
22a NAME OF RESPONSIBLE INDIVIDUAL James Lewkowicz	22b TELEPHONE (Include Area Code)	22c OFFICE SYMBOL GL/LWH

lower than 1 nm^2/Hz at 1 Hz and a fairly smooth decay proportional to f^{-4} per decade up to 40 Hz, leading to a value of 10^{-4} nm^2/Hz at 10 Hz and 10^{-5} nm^2/Hz at 20 Hz. Diurnal variations due to industrial noise sources such as saw mills are mostly found in the 4 Hz to 10 Hz band. Compared to Scandinavia, the noise level in Central Europe is comparable or even lower for frequencies about 1 Hz but it is about a decade higher at 10 Hz and above.

The spatial correlation properties of noise and signals were investigated with data from a temporary 9-element array with a diameter of 3 km. In the 1 Hz - 2 Hz band, the noise coherence values drop to 0.25 at interstation distances of 800 m, and in the 2 Hz - 4 Hz band at interstation distancies of 400 m, respectively. There is no clear evidence for a negative noise correlation distance at these frequencies.

The relative amplitudes of regional phases, i.e. Pn,Pg,Sn, and Lg are strongly path-dependent. From northern azimuths Pg- and Lg-phases are dominant with an optimum signal-to-noise ratio in the frequency band below 10 Hz. For southern and south-western bearings, which correspond to Alpine wave-paths, Pn and Sn show the largest amplitudes with a very high frequency content up to 50 Hz.

Signal coherence in the same frequency bands as they were used for noise correlation, proved to be excellent (> 0.9) for all regional phases over the 3 km aperture of the test-array.

The final configuration of the new regional array in the BF-area - named GERESS - has been selected as a slightly enlarged NORESS-type ring geometry with an innermost radius of 200 m and a largest radius of about 2000 m.

Table of Contents

iii

I. Design and Siting of a New Regional Seismic Array in Central Europe

1. Introduction

Since tne establishment of the Graefenberg (GRF) array in 1980, array research in Germany was focused on teleseismic data due to the broadband instrument response with a high-cut filter at 5 Hz and an average station distance of more than 10 km. In recent years, an increased interest emerged in the evaluation of high-frequency signals from events at regional distances. Small-size and many element arrays like NORESS have proven capable of taking advantage of the very efficient propagation of high-frequency seismic phases. Together with a similar recently installed array in Northern Norway (ARCESS), the proposed array in Southern Germany (tentatively named GERESS = GERman Experimental Seismic System) would built an array network with nodes at roughly 1000 km intervals. Such a configuration is particularly suited for automated location procedures applying antenna theory and it is relevant in view of a possible deployment of "in-country" seismic systems for a surveillance of a possible future nuclear test ban treaty.

In Central Europe a siting survey has carefully to investigate noise sources due to the dense population, high traffic, and various industries. Apart from the local noise conditions, sufficient seismic signals from different azimuths should be recorded and evaluated to assess the propagation of high-frequency signals, especially across tectonic boundaries like the Tornquist-Teisseyre suture between the Russian Platform and Western Europe or the influence of the Alps on signals originating from the Mediterranean earthquake region.

After describing the site survey in chapter 2, a typical noise power spectrum, taken from data recorded in Southern Germany, will be compared with spectral noise conditions in Scandinavia. A low-noise profile is only one condition for a reasonable array site. Equally important is the transfer function of the receiver crust which influences the signal characteristics and the signal to noise ratio. Unlike the fairly homogeneous Scandinavian shield the geologic conditions in Central Europe are rather complex reaching from thick alluvial sediments in the North German Basin which is separated by the Variscan mountain front from the Alpine foreland to the Alps itself. Besides the Black Forest at the Eastern Rhinegraben, the Bavarian Forest (BF) area at the border to Czechoslovakia and Austria represents the largest outcropping crystalline block in Germany. This region is principally suited for an array installation of the proposed kind as has been demonstrated by the excellent detection capabilities of conventional seismic stations in Austria and Czechoslovakia.

In chapter 3 signal and noise correlation measurements in the BF-area will be described which are used as important constraints for the array design. For this purpose a nine-element array was operated temporarily around the site where the lowest noise values were found previously.

From these measurements the final geometry of the GERESS array was determined and its array response is compared with the existing Scandinavian arrays.

A preview on the installation schedule of the new array will be given in chapter 4 including information on the type of instruments and the data acquisition units used.

2. Site Survey.

Field work has been carried out initially in October 1987 and then continuously from April to July 1988. Some additional data have been collected later in 1988 to prove the long-term variability of noise conditions and to calibrate the results with data from well-defined events (e.g. JVE-explosions in Nevada and Kasachstan).

Unlike NORESS which is built within a subarray of the large teleseismic NORSAR array, it was not possible to collocate the new high-frequency array with an existing GRF-subarray because the latter teleseismic broadband array is placed on a sedimentary column which strongly attenuates high frequencies. As shown in Figure 1, the new array site is situated about 150 km east of the GRF-array location.

The noise measurements concentrated on the outer Bavarian Forest just east of a major fault line named the "Pfahl" which separates the Bohemian Massif from the western Molasse - a quaternary and tertiary sedimentary basin in the Alpine foreland. The advantage of the BF-area is its geological setting (crystalline outcropping rocks) and the low population density. The landscape is mostly mountainous up to 1200 m elevation. Nearly all recording sites were situated in extensive forest areas to minimize cultural noise and instruments were installed on granite or gneiss rocks to record high frequencies, especially from events at regional distances. Due to the installation on the surface, the seismometers were quite sensitive to wind noise but for technical and financial reasons no other arrangement was feasible. Detection capabilities derived from noise estimates of these data should represent conservative values.

For survey purposes three portacorders with direct recording were used. In case of favourable places one of three digital data acquisition systems was installed for a time period of several weeks. The digital systems were PCM recording instruments of Lennartz 5800 type with the following specifications:

ADC - 66 dB resolution, gain ranging -- 126 dB dynamic range,
sampling frequency -- 250 Hz, and low-cut filter -- 44 Hz, 6 pole Bessel.

Each PCM system was equipped with three vertical short-period seismometers (1 Hz Geotech S-13) which were installed at distances between 100 m and 300 m to avoid false alarms by coincidence triggering.

Very soon the site survey concentrated on an area which is closest to the CSR border. Very few roads, low population density, and extensive woodland offered adequate pre-

conditions for seismic installations. The first station was established in April 1988. It was placed on weathered granite. Later, two other stations were established on gneiss. During the JVE-experiment an additional station was installed on granite at a place where adequate housing and power facilities were available to operate a hub for a temporary small array subsequently. All four sites were located within a radius of 5 km. Portacorder records showed a generally low noise background and especially a small day-to-night variation. The only obvious disadvantage appeared to be some saw-mills which generated monochromatic seismic noise during working hours.

For comparison some noise samples have been taken at the Graefenberg array (station B5) which confirmed earlier measurements showing relatively high cultural noise levels.

Finally during a short trip to Norway in October 1988, some recordings were made at NORESS to get a direct comparison of noise values by using the same data acquisition system and - more important - the same processing procedure as for data from the area under investigation in Germany.

The processing of field data included several steps. At the beginning the PCM field tapes had to be converted to standard 9-track IBM-compatible format.

Having recorded the field data in event mode the pre-event window can be used for noise evaluation. There are many well-established methods to estimate the power spectral density of stationary time series (e.g. Oppenheim and Schafer, 1975; Welch, 1967). In this report the following procedure was applied : Altogether 20 seconds of the pre-event window were divided into 19 blocks of 2 seconds length each with an overlap of one second. Each data block was padded with zeros to get a FFT-transformation length of 2^{10} reminding that the original sampling frequency of the field data was 250 Hz. The 19 raw Fourier spectra were averaged to lower the variance without affecting stationary noise peaks. The final step includes an average of 12 noise spectra from each station and a plot of the mean values and their standard deviation.

The noise spectra were calculated separately for day and night. They cover the whole time period during which the corresponding station was operating. By that procedure, working hours, weekends, and different weather conditions are included in the noise estimate.

Figure 2 shows a typical noise spectrum for the BF-area. The solid line represents the average and the dotted lines one standard deviation calcuiated as explained in the preceding text. The estimate includes data from summer and from winter when the ground was covered with snow. In the individual spectra no significant difference could be observed. The spectrum shows a continuous slope with a small variance and the 2 Hz peak, commonly observed at stations in Central Europe, can only be recognized during night times. The day spectrum is dominated by a noise maximum at 4-5 Hz which is supposed to originate from a saw mill at a distance of a few kilometers. Apart from this peak the noise spectrum shows a smooth decay proportional to f^{-4} from 1 Hz to 30 Hz and a small standard deviation. Taking into account that the recording time covered nearly a period of four months, this area seemed to be promising for an array installation.

To secure this suggestion, three other sites were explored in the vicinity. Indeed, their spectra looked very similar and confirmed the favorable opinion about the area.

To put our noise results from the Bavarian Forest into proper place, additional data were collected at the Graefenberg array and at NORESS. GRF can be regarded as a typical Western European site whereas NORESS is well known for its excellent noise conditions being situated on the Scandinavian shield.

At day the GRF-spectrum (Figure 3) shows much larger noise values than in any of the BF-spectra. The influence of industry and traffic is especially pronounced as seen in the large variation. The night-spectrum at GRF looks similar to the BF-spectra between 1 Hz and 8 Hz. For higher frequencies the different geological setting (sediments) causes still higher noise values. From this direct comparison we can conclude that the BF-area exceeds most other places in the FRG - and certainly GRF - as a potential site for an establishment of a high-frequency array.

More interesting is the comparison of the proposed Bavarian area with NORESS. The spectra shown in Figure 4 were calculated from a 24 hour noise sample analyzed with the same procedure as described above. There are remarkable differences in the noise spectra. For low frequencies around 1 Hz NORESS clearly suffers from the influence of the Norwegian coast which results in an order of magnitude higher PSD-values compared to the Bavarian Forest area ($10nm^2/Hz$ to less than $1nm^2/Hz$). Apparantly these microseisms lead to a steep slope of the spectrum proportional to f^{-5} up to frequencies of 2 - 5 Hz. For higher frequencies this slope is flattened and becomes comparable to the f^{-4} fall-off at the BF-area. The absolute noise values at 10 Hz and 20 Hz are certainly lower at NORESS but also some influence of industrial noise between 5 Hz and 8 Hz can be identified in the spectrum. According to personal information from the NORSAR staff, there is also a saw mill operating at a distance of roughly 10 km from the NORESS array.

In summarizing the comparison between NORESS and the BF-area we found higher noise values at NORESS for frequencies below 2 Hz and higher noise values at the BF-site for frequencies between 2 Hz and 20 Hz. The consequence of this difference in terms of detection capabilities can only be evaluated comparing events recorded at both arrays.

3.   Array Design.

The GERESS array is planned as part of a multi-array network which will include the NORESS and ARCESS arrays in Scandinavia. Consequently the design philosophy followed those existing arrays and it is well documented in several publications (e.g. Followill and Harris, 1983, Mykkeltveit, 1985).

The geometry of these regional arrays is based on concentric rings spaced at log-periodic intervals in radius R, following the relation

$$R = R_{min} \alpha^n , n = 0, 1, 2, 3 \tag{1}$$

with 3, 5, 7, and 9 elements in each ring, plus one in the center.

With an odd number of elements in each ring, the corresponding coarray samples the local wavefield in the least redundant way. In this sense, such a configuration comprises subsets of sensors with very different intersensor separations implying that both high-frequency and low-frequency regional phases can be well enhanced by appropriate subsets of the array (Kvaerna, 1989).

An essential aspect of the array design is the supposition that intersensor spacings should correspond to maximum correlation for the signal and minimum correlation for the noise. Seismic signal and noise characteristics are influenced not only by the geologic formations of the array site, but also by the type and strength of sources and their locations with respect to the array. Consequently, determination of the actual values of the parameters in (1) for a specific site is to be based on observed signal and noise correlations.

Our correlation curves are derived from measurements made with a 9-sensor test-array operating from December 1988 to April 1989 in the BF-area where we found the lowest noise conditions earlier. The configuration of the test-array and its corresponding coarray are shown in Figure 5. Interstation distances range from 200 m to 3000 m. Short-period instruments (Geotech S-13) were placed in small vaults of 2 m to 4 m depth. At this depth the overburden of soil was penetrated in general, but the underlying crystalline bedrock was still heavily weathered. The main advantage of the vault installation was to avoid wind noise induced by the surrounding forest.

New digital data acquisition systems (Geotech PDAS-100) were used for recording which sampled at 100 Hz with a resolution of 16 bits. Data synchronization was controlled by an external radio signal (DCF-77). The test-array operated in detector mode with a conventional STA/LTA-detector, recording length was generally 3 min with a pre-event window of 30 sec.

Figure 6 shows an average noise power spectrum of the test-array. The trend and absolute values coincide quite well with the results of the previous site survey (Figure 2) confirming confidence that the selected area is suited for an array installation. Noise correlations were calculated from the pre-event window of 35 different events covering the whole recording period. The raw data were bandpass filtered between 1 Hz - 2 Hz and 2 Hz - 4 Hz, respectively with a two-pole, both-directional (zero-phase) Butterworth filter.

The correlations are expressed by

$$c = \frac{\sum\limits_{i=1}^{N} (x(i) - \bar{x}) (y(i) - \bar{y})}{[\sum\limits_{i=1}^{N} (x(i) - \bar{x})^2]^{1/2} [\sum\limits_{i=1}^{N} (y(i) - \bar{y})^2]^{1/2}} \qquad (2)$$

x(i) and y(i) are sample values for sensor x and y, N is the number of samples and $\bar{x}$ and $\bar{y}$ the mean values of the N samples.

The window length was taken as 10 sec (1000 samples). The correlations were calculated for all 36 different combinations of seismometer pairs, i.e. all the coarray points (Figure 5).

Our results are summarized in Figure 7. In the lower half, the individual correlation values are shown within the 1 Hz - 2 Hz passband together with a smoothed average. The large scatter in the data may reflect as well the short window length as also some problems with the synchronization during data acquisition. On the other hand, the solid line representing an average trend, indicates a quite reasonable behaviour, especially when we add the upper half of the figure which presents the corresponding data in the 2 Hz - 4 Hz passband. Defining the correlation length as that station separation for which the noise coherence drops below 0.25, we get a correlation length of about 800 m for the 1 Hz - 2 Hz passband and 400 m for the 2 Hz - 4 Hz passband. In a wide sense, this result is consistent with values found for NORESS. The main difference to noise correlation studies in Scandinavia is the absence of a significant minimum. The noise correlation curves for the BF-area show a smooth decay without a pronounced negative correlation distance. If this preliminary result will be confirmed by a comprehensive analysis of the future array data there could be various explanations: firstly, the isotropic noise model (Backus et al, 1964) might not be applicable in an azimuthally heterogeneous geologic region like Central Europe or alternatively, the minimum in noise correlation for Scandinavian stations originates from directional propagating noise which could be higher mode microseisms. The higher noise level at low frequencies which was earlier mentioned in comparing Figures 2 and 4 supports the latter hypothesis.

However, in the final design of the NORESS array, not much use has been made of the noise minimum because in the range of interesting frequencies the corresponding interstation distance varies and optimum geometries would be vastly different (Mykkeltveit, 1985).

As a consequence of the noise correlation curves, the minimum station distances for the planned GERESS array could be slightly increased in comparison to NORESS taking into account that the detection window with the best signal to noise ratio is generally shifted to lower frequencies for stations in Central Europe. Whether this can lead to a larger overall aperture depends on signal correlation. Figure 8 shows a regional earthquake recorded by the test-array in the BF-area. It is a mining-induced event originating at Lubin in the Polish copper mines at a distance of 360 km from the test-array. Besides the first arriving Pn-

phase, we recognize Pg and Lg wavetrains as dominant signals, a typical picture for events from northern or northwestern azimuths.

In Figure 9 the signal spectra are plotted together with the background noise. Although all three phases stay above the noise level up to frequencies of 30 Hz, the best signal to noise ratio is obviously in the 1 Hz - 5 Hz band. Certainly this figure changes with azimuth and at the BF-site there are special wave paths along the Alps where we see much higher signal frequencies and Pn and Sn become the dominant phases. But in general, frequencies below 10 Hz are most important for the evaluation of regional waves within 1000 km distance.

Signal correlations were calculated with the same procedure which was used to establish the noise correlation curves. Time shifts have been performed with an optimum line-up of peaks and troughs at the different sensors, and 1 sec or 2 sec windows of each phase were analyzed. In Figure 10 the signal correlation curves are shown for the Pn, Pg, and Lg phases using the same 1 Hz - 2 Hz and 2 Hz - 4 Hz passbands as for the noise correlation. Additionally the noise correlation is marked in Figure 10 by stars which represent the plus/minus one standard deviation range. As can be seen from the figure, all signal correlation values stay above 0.9 for all interstation distances out to 3000 m with the exception of the Lg phase in the 2 Hz - 4 Hz passband. Similar signal correlation curves were obtained analyzing a number of regional events from different azimuths.

From these measurements it was concluded to maintain the general geometry of the NORESS array but to enlarge it for the planned GERESS array by a factor of 4/3 which results in a radius of 200 m for the innermost ring and about 2000 m for the outermost ring, respectively. In conclusion, the parameters in equation (1) for the concentric array layout were specified as $R_{min} = 200$ m and $\alpha = 2.15$.

The final siting of the 25 array elements had to take some local geologic and topographic peculiarities into account. In addition some restrictions, imposed by the forest authorities had to be considered. Nevertheless the final configuration, displayed in Figure 11 is still sufficiently close to the concentric ring concept and consequently the GERESS array will represent a uniform element in the multi-array network including ARCESS and NORESS, the arrangement of the latter is displayed in Figure 12 (left side).

For comparison the array responses of GERESS and NORESS are plotted on the right side of Figure 11 and Figure 12, respectively.

Due to the larger aperture, the main lobe is smaller than the NORESS main lobe but on the other hand minor side lobes can be seen in the reject region in the wavenumber domain. For a fixed number of sensors this reflects the wellknown trade-off between resolution and aliasing properties. Whether the superior resolution of the GERESS array will lead to improved location and phase identification capabilities has to be postponed until the new array becomes operational. An essential aspect of the array design using the concentric ring concept deals with the uniform average of the coarray domain. As shown in Figure 13, the distribution of coarray points is very similar for GERESS and NORESS and different subgeometries will achieve the optimum signal to noise gain in different frequency bands

and with different wavelengths.

4.   Discussion and Preview.

Since several conflicting demands can be put on array performance, it is difficult to make general comparisons of array design. For the regional array concept developed at NORSAR, the underlying objectives are determined in the context of a monitoring system for a future nuclear test ban treaty. A special aspect of such a system is the identification of weak seismic events using high-frequency data (Archambeau et al, 1986). As a prototype array NORESS has demonstrated promising capabilities. It is however difficult to generalize NORESS results because this array is located within on old shield region with high Q values. Additionally the natural seismicity within regional distances is relatively weak. The GERESS array, on the other hand, will be situated in a rather complex geologic and geotectonic environment where high Q and low Q wave paths drastically change with azimuth. The array site is surrounded by various artificial seismic sources like quarries and mines but more important, the Alpine earthquake belt and the Mediterranean earthquake zone lie within about 1000 km distance. Consequently, the number and nature of regional seismic events recorded at GERESS should be more manifold than at any recording site in Scandinavia. For optimum performance of a seismic surveillance system, detection, location, and identification of events at low signal to noise ratios is important. It will be interesting to observe whether automatic procedures developed for these tasks at NORSAR, can be adapted to the seismic situation in Central Europe. In any case, the use of arrays as components of a global seismic network can be evaluated more realistically the more the arrays and their recordings represent typical conditions of a global monitoring system.

In summer 1990 the GERESS array should become fully operational. After the final configuration was defined, excavation of vaults and trenching of cables started in October 1989. Figure 14 shows that in addition to the 25 vertical instruments four sites will include horizontal components. All these are short-period (1 Hz) Geotech GS-13 type instruments sampled at 40 Hz. The array will be supplemented by one three-component set of GS-13's sampled at 120 Hz and these instruments will be collocated with a three-component set of broadband seismometers (BB-13) sampled at 10 Hz. The sites were selected to have an option for a good three-component subarray taking into account the site-specific noise conditions. In contrast to vault A2, the central vault NU did not reach the basement rock and it appeares to be noisier than the average array station. Site C2 is very close to the hub facility and allows easy access which might be favorable in case of modifications at the broadband or high-frequency instruments. As all sites are equipped with data acquisition units using 24 bit A/D converters, the data will provide sufficient resolution and dynamic range to evaluate small-size and large-size earthquakes simultaneously. For interesting events, data from the three-component high-frequency and broadband instruments can be pieced together to study the seismic wavefield in a very broadband sense.

The GERESS array will be installed and operated as a joint project of the Geophysical Laboratory of Southern Methodist University Dallas and the Geophysical Institute of Ruhr-University Bochum. Data will be available at NORSAR and Bochum.

References.

Archambeau, C.A., J.F. Evernden, and E. Cranswick (1986). An evaluation of seismic decoupling and underground nuclear test monitoring using high frequency seismic data. Rev. of Geophys. 24, 143-215.

Backus, M., J. Burg, D. Baldwin, and E. Bryan (1964). Wide-band extraction of mantle P waves from ambient noise. Geophysics 29, 672-692.

Followill, F. and D. Harris (1983). Comments on small aperture array designs. Internal report, Lawrence Livermore National Laboratory.

Kvaerna, T. (1989). On exploitation of small-aperture NORESS type arrays for enhanced P-wave detectability. Bull. Seism. Soc. Am. 79, 888-900.

Mykkeltveit, S., K. Astebol, D.J. Doornbos, and E.S. Husebye (1983). Seismic array configuration optimization. Bull. Seism. Soc. Am. 73, 173-186.

Mykkeltveit, S. (1985). A new regional array in Norway : Design work and results from analysis of data from a provisional installation, in The VELA Program. A Twenty-Five Year Review of Basic Research. A.U. Kerr, Editor, Defense Advanced Research Projects Agency.

Oppenheim, A.V. and R.W. Schafer (1975). Digital Signal Processing. Prentice Hall Inc., Englewood Cliffs, New Jersey.

Welch, P.D. (1967). The use of fast fourier transform for the estimation of power spectra: A method bases on time averaging over short, modified periodograms. IEEE Transaction Audio Electroacoust. AU-15, 70-73.
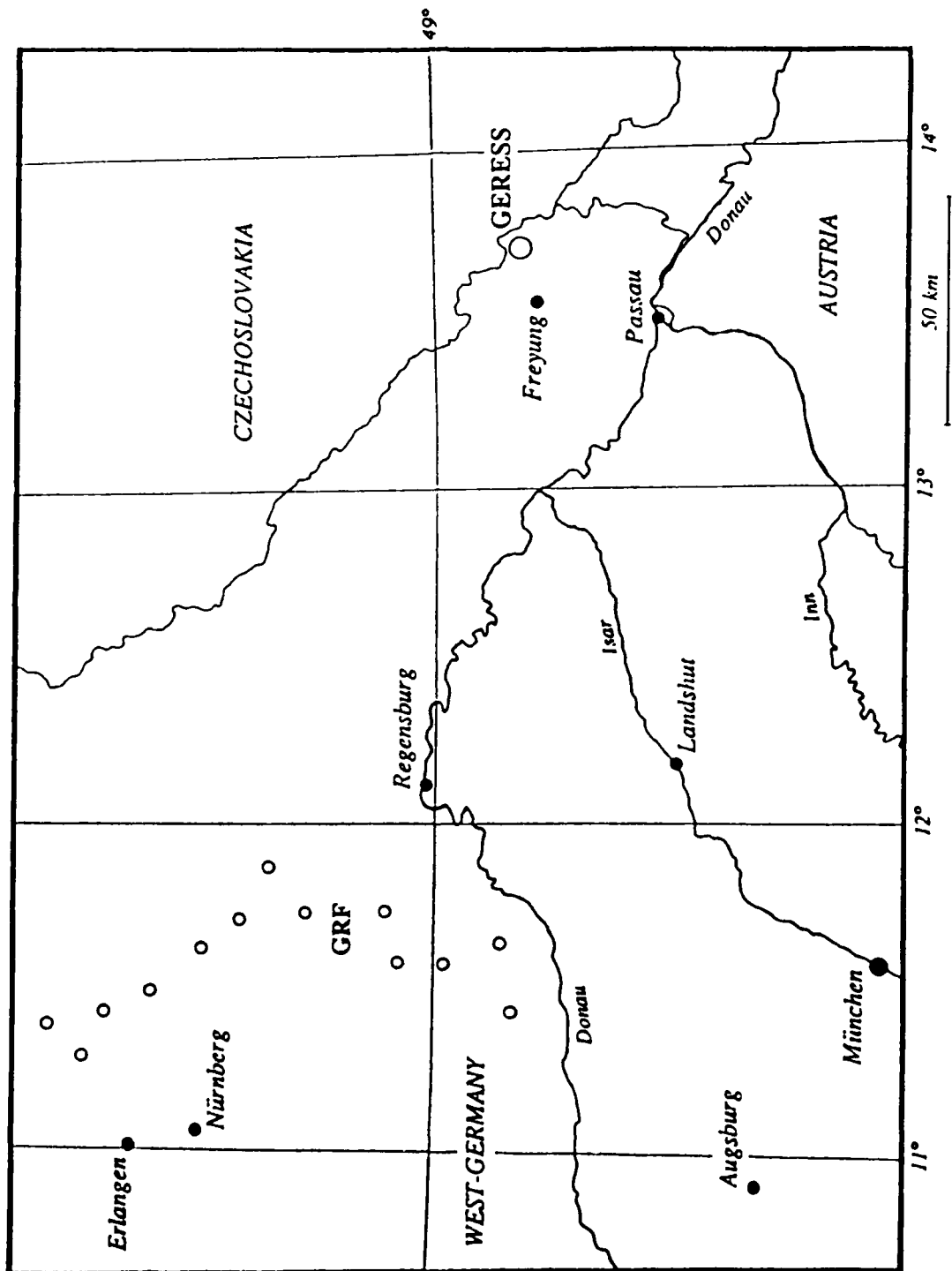
Fig. 1 : Geographical location of the existing teleseismic GRF-broadband array and the planned regional GERESS array.
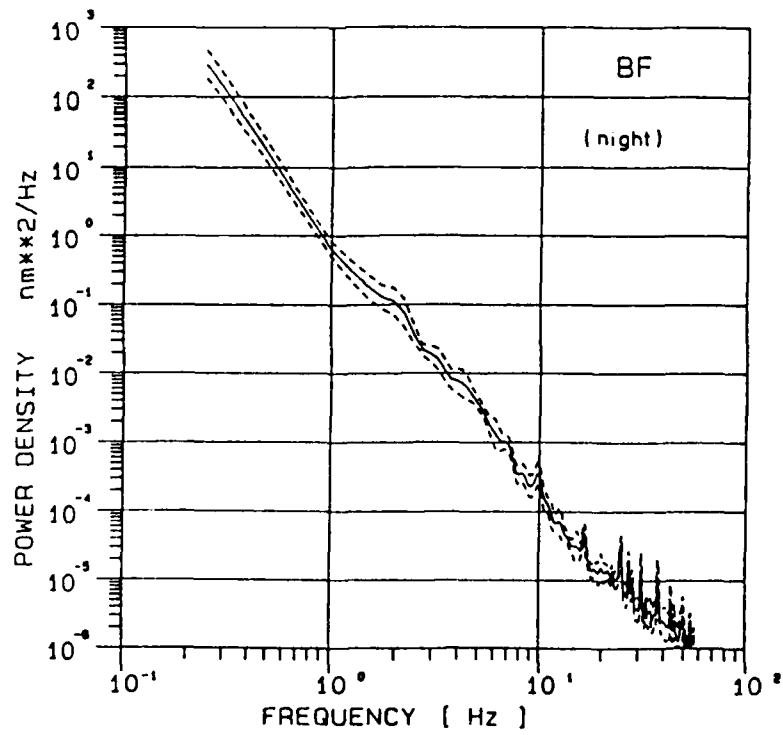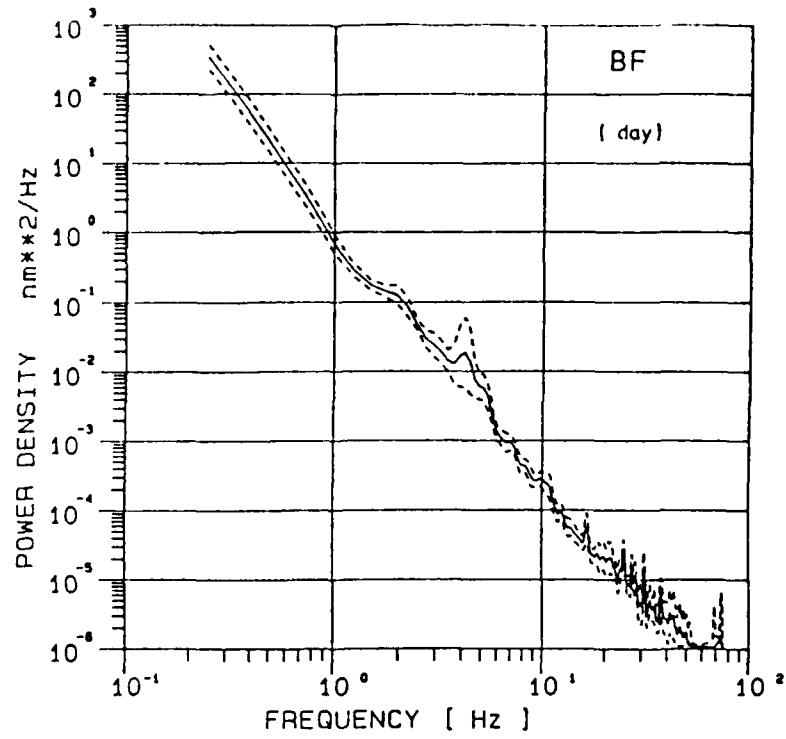
Fig. 2 : Displacement power spectra of noise in the Bavarian Forest (BF) area for day
and night. Solid line represents an average of 12 different data samples,
dotted lines mean plus/minus one standard deviation
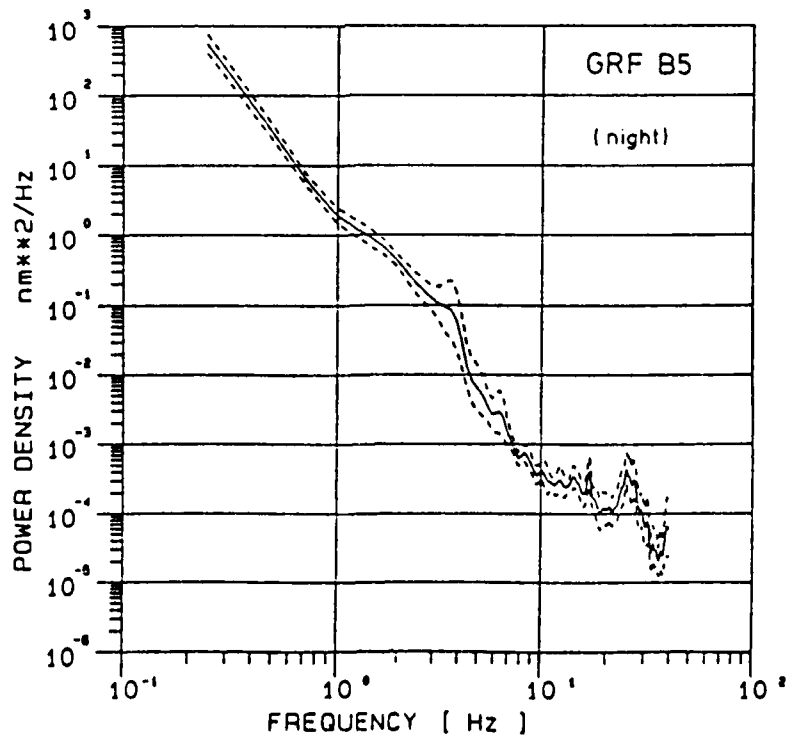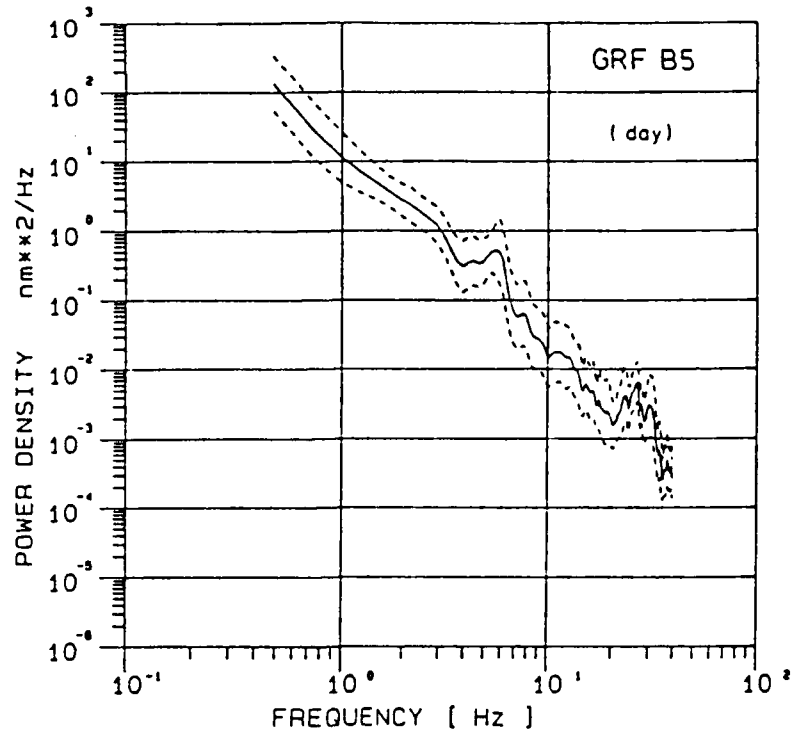
Fig. 3 : Displacement power spectra of noise at the GRF-array (site B5).
For explanation see Fig. 2.
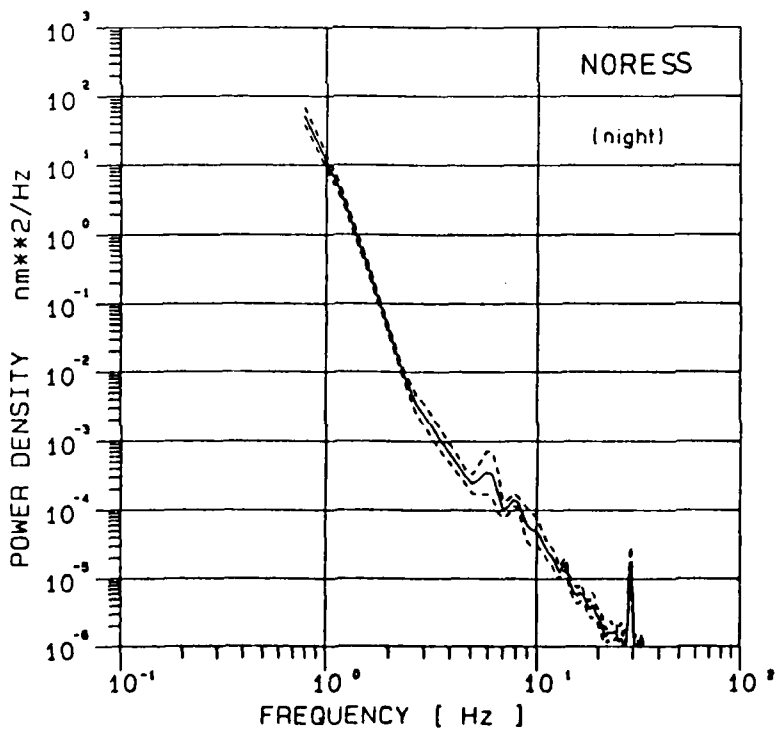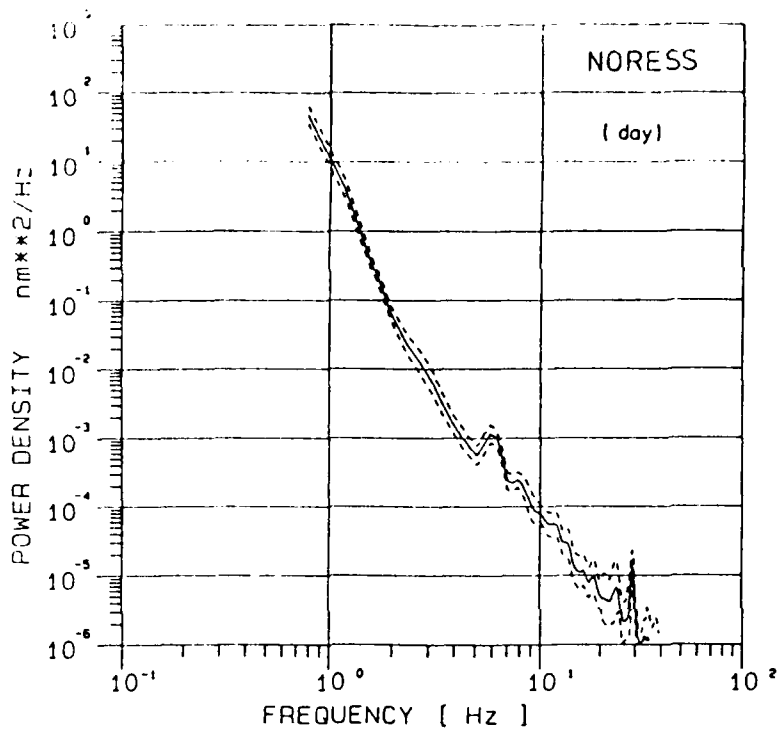
Fig. 4 : Displacement power spectra of noise at NORESS (site C4).
For explanation see Fig. 2.
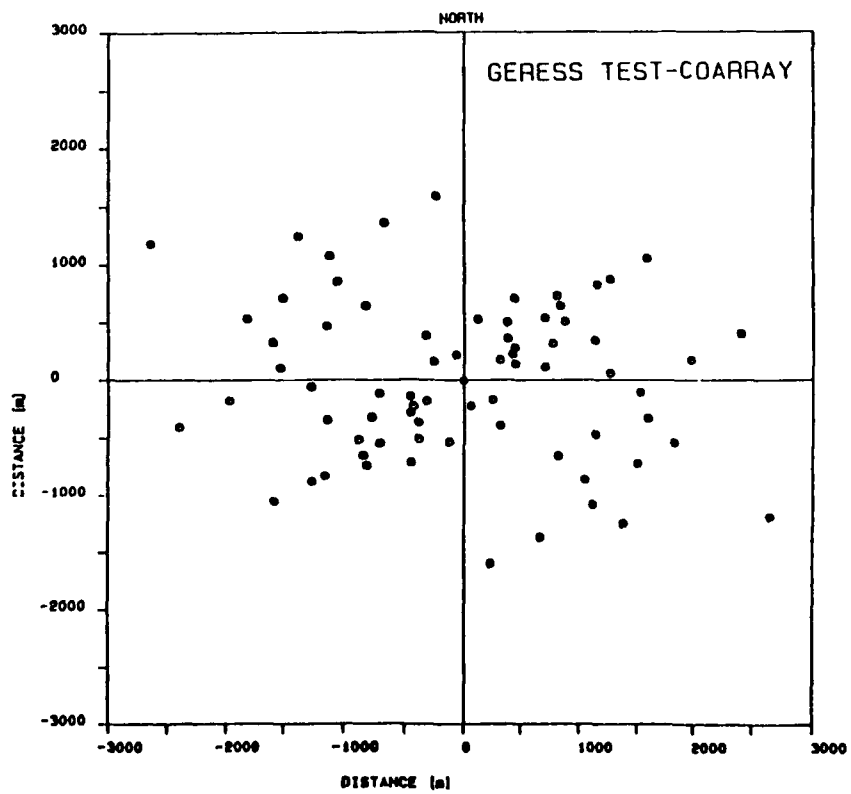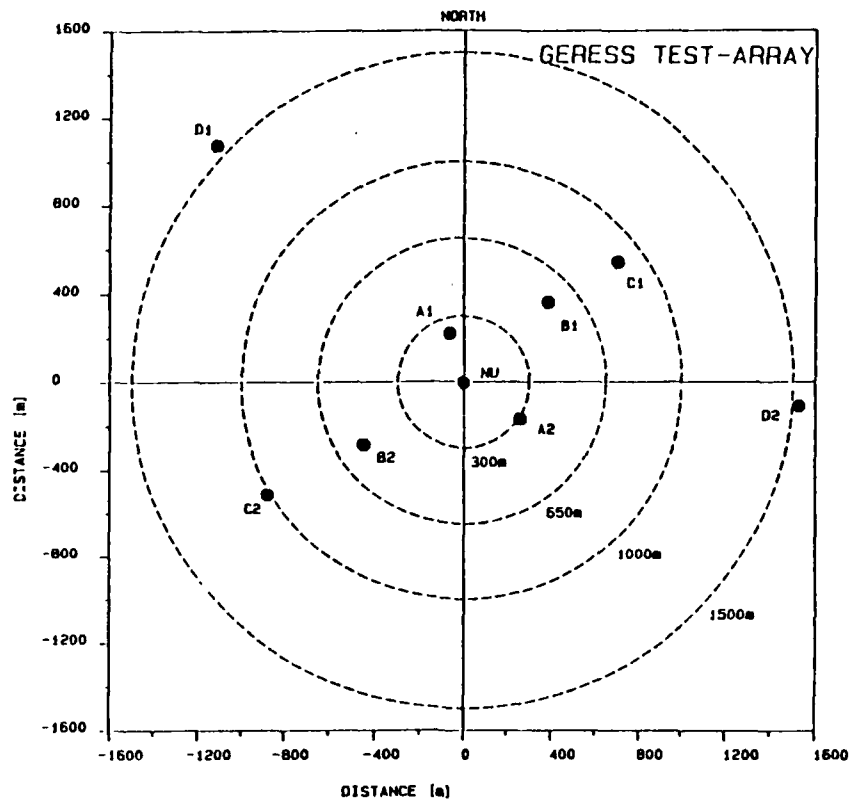
Fig. 5 : Nine-element test-array in the BF-area. Coordinates of central vault: 48.845N, 13.700E. The coarray on the right side shows all interstation distances in vector space.
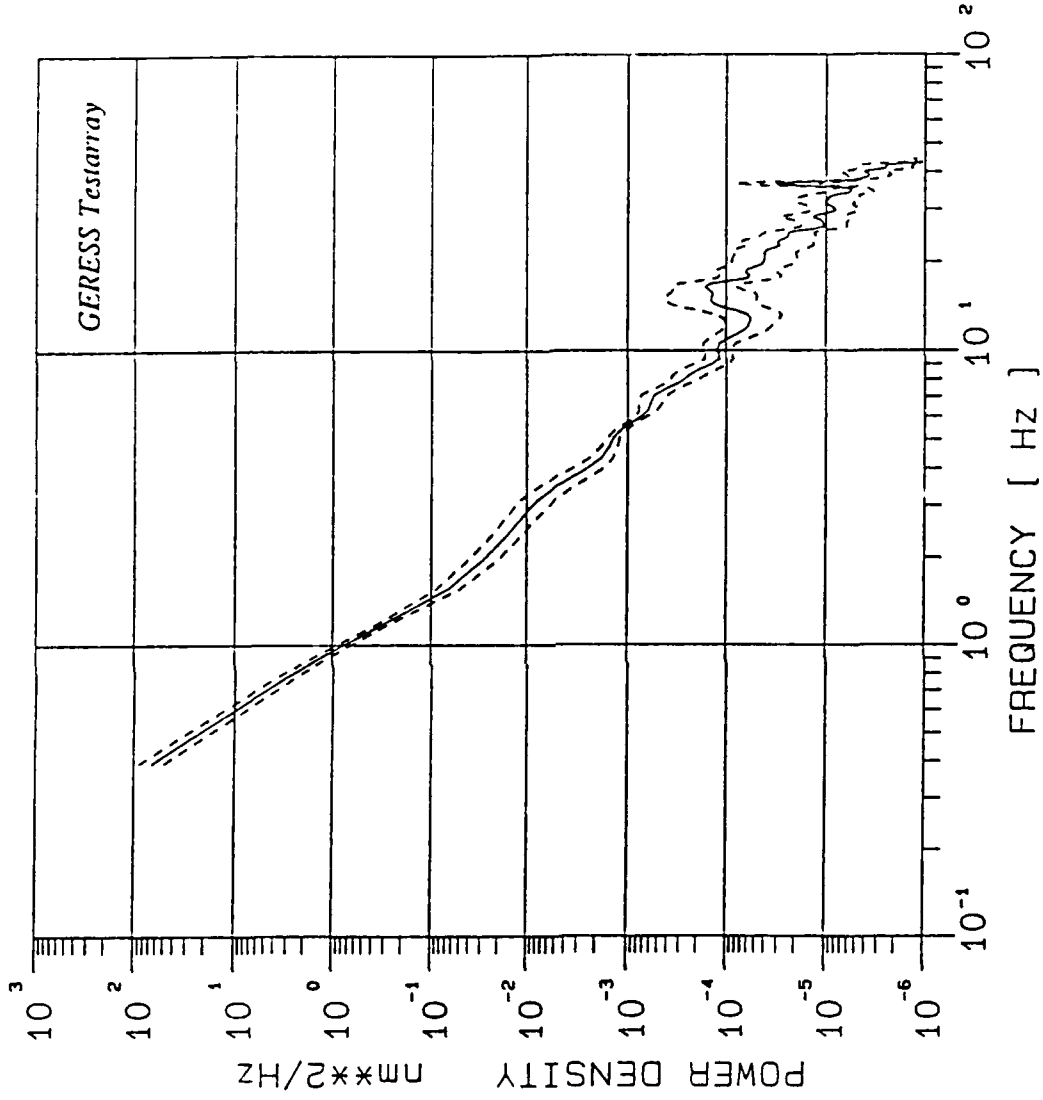
Fig. 6 : Average displacement power spectra of noise for all elements of the test-array in the BF-area. Dotted lines mean plus/minus one standard deviation.
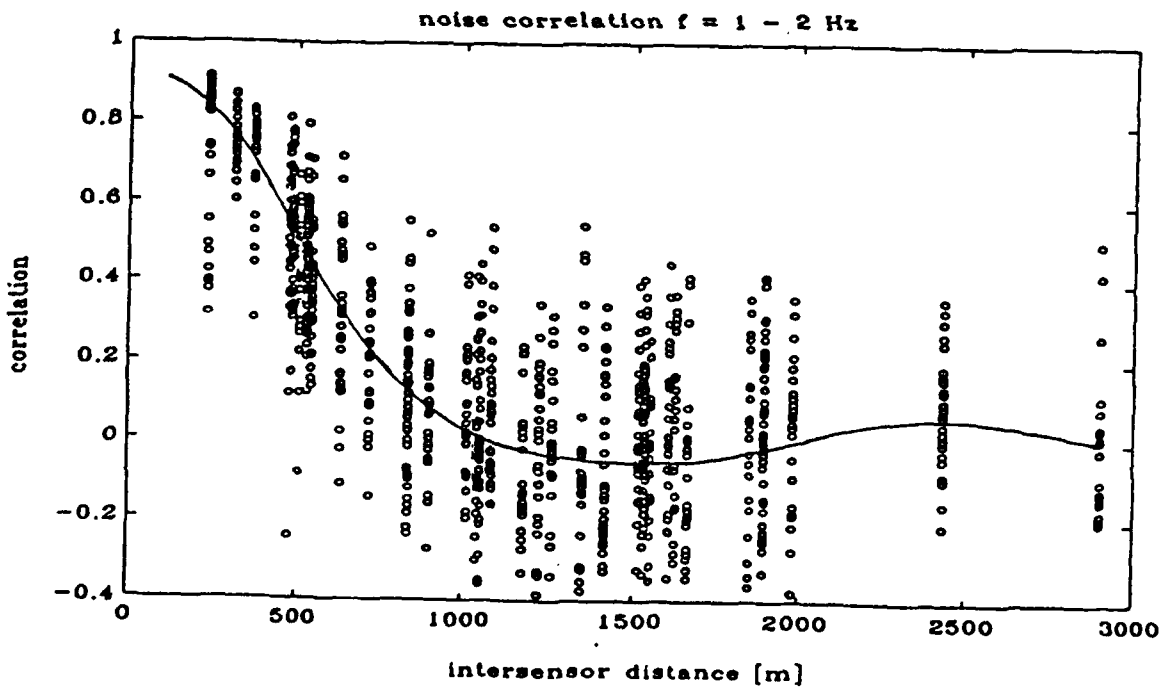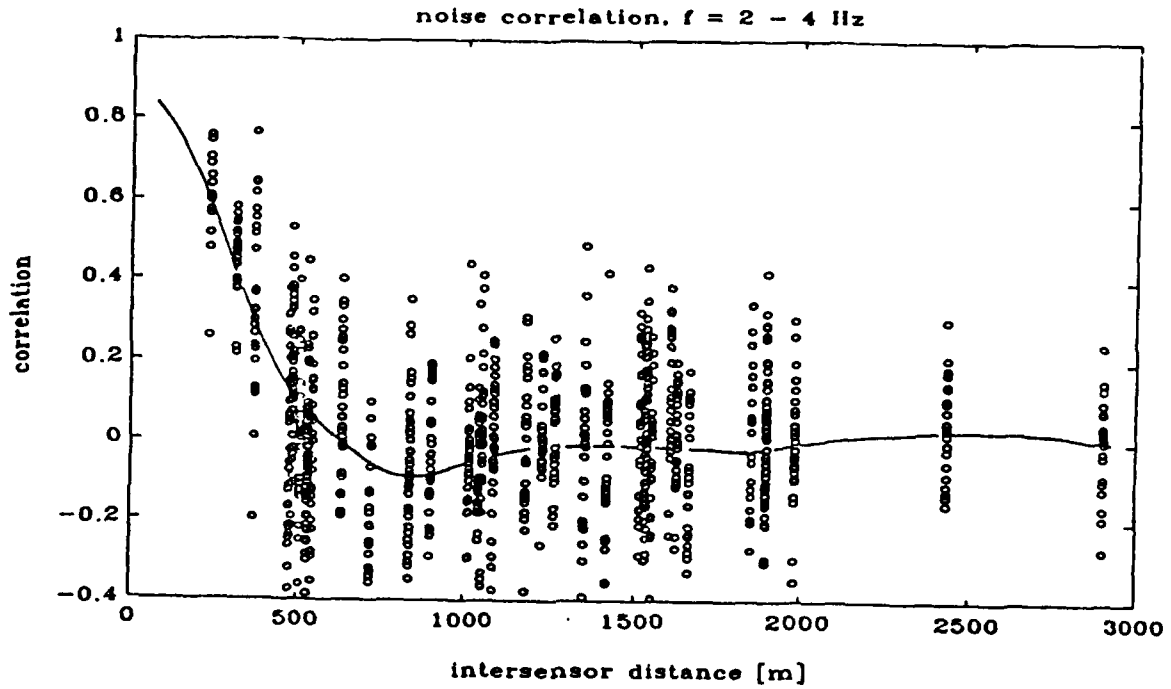
Fig. 7 : Noise correlation values within the test-array. (top : prefilter 2 Hz - 4 Hz, bottom : 1 Hz - 2 Hz passband) The solid lines represent a smoothed average curves.
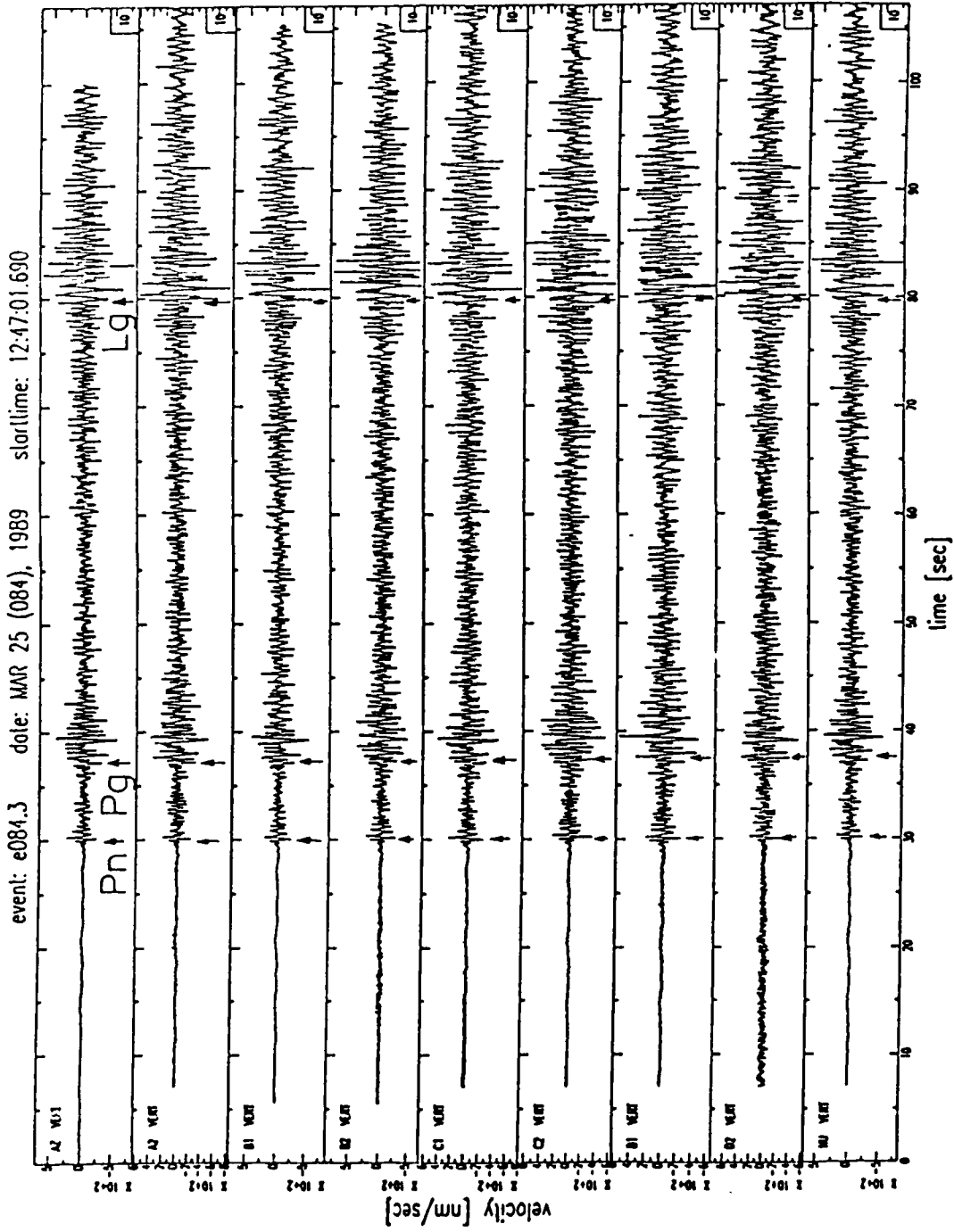
Fig. 8 : Test-array data (9 traces) of an ml=3.8 (KBA) earthquake near Lubin (Poland). Epicentral distance is 354 km. Prominent regional phases are marked as Pn, Pg, and Lg.
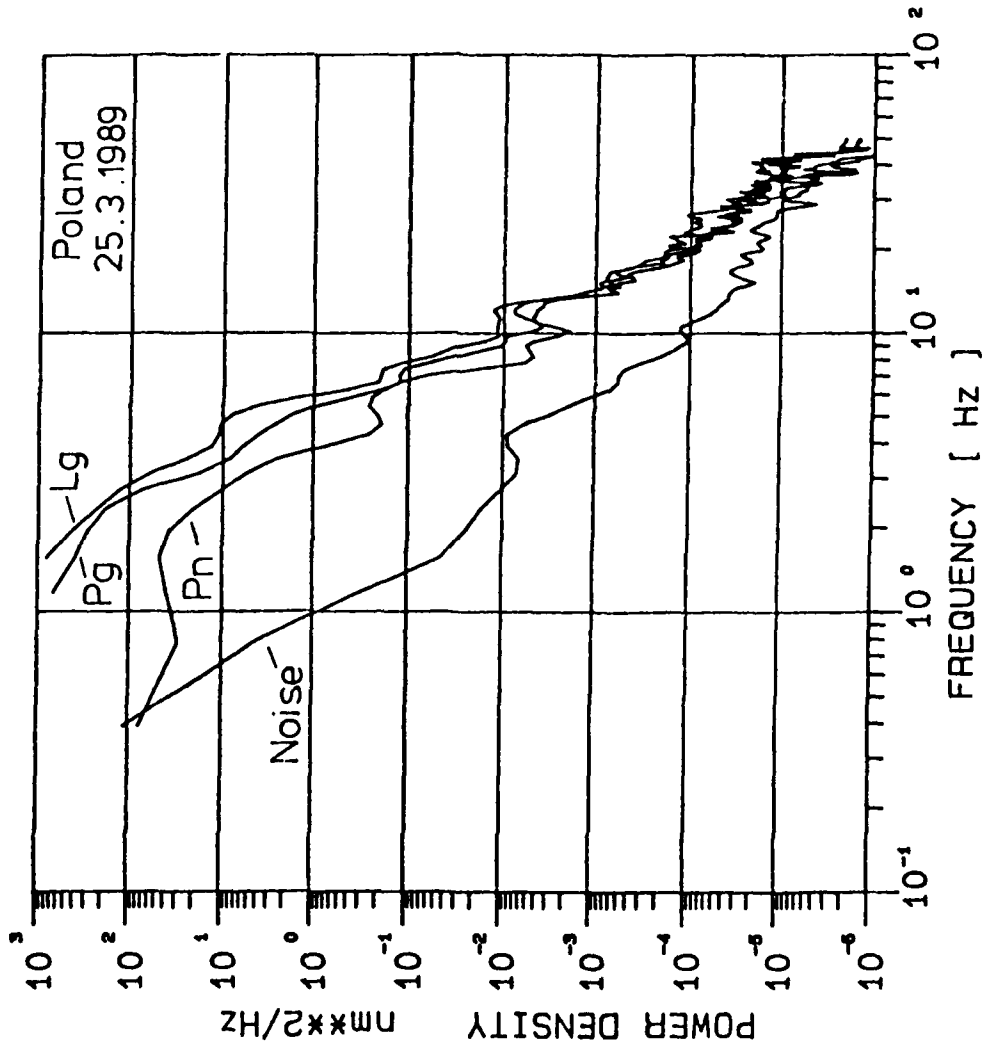
Fig. 9 : Signal and noise power spectra for Lubin event for site A1 from Fig. 8.
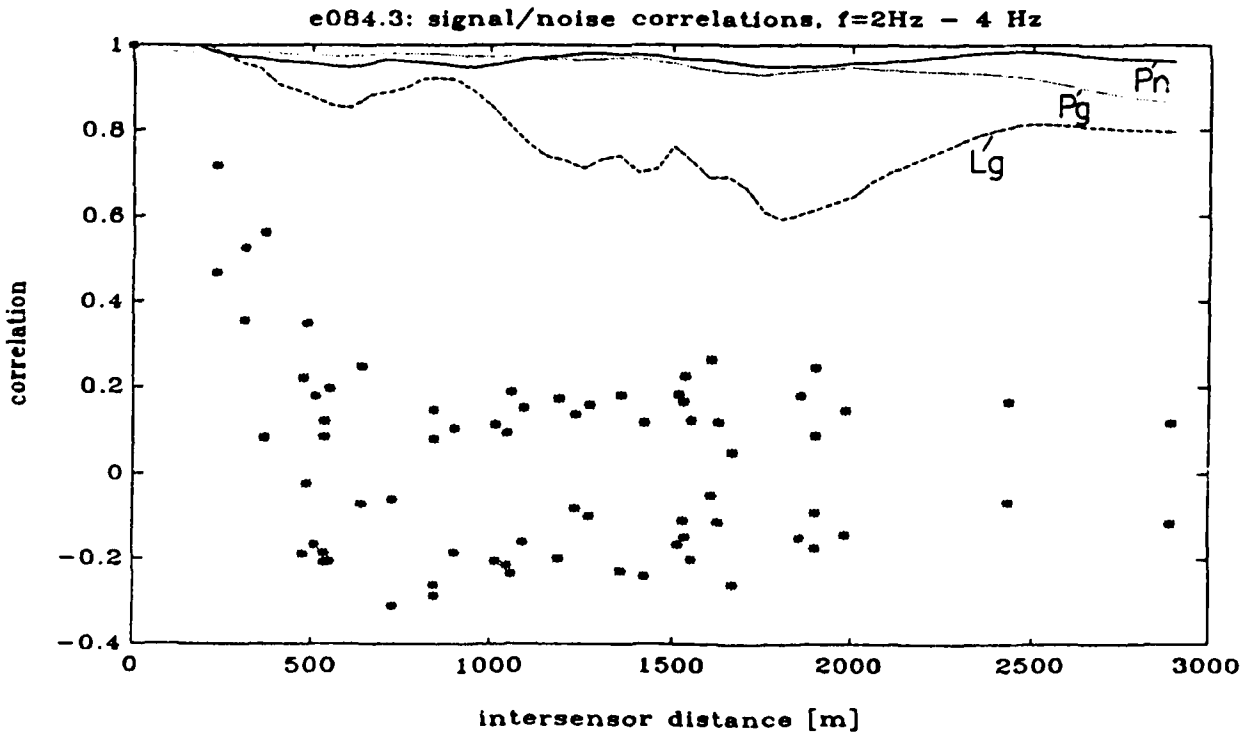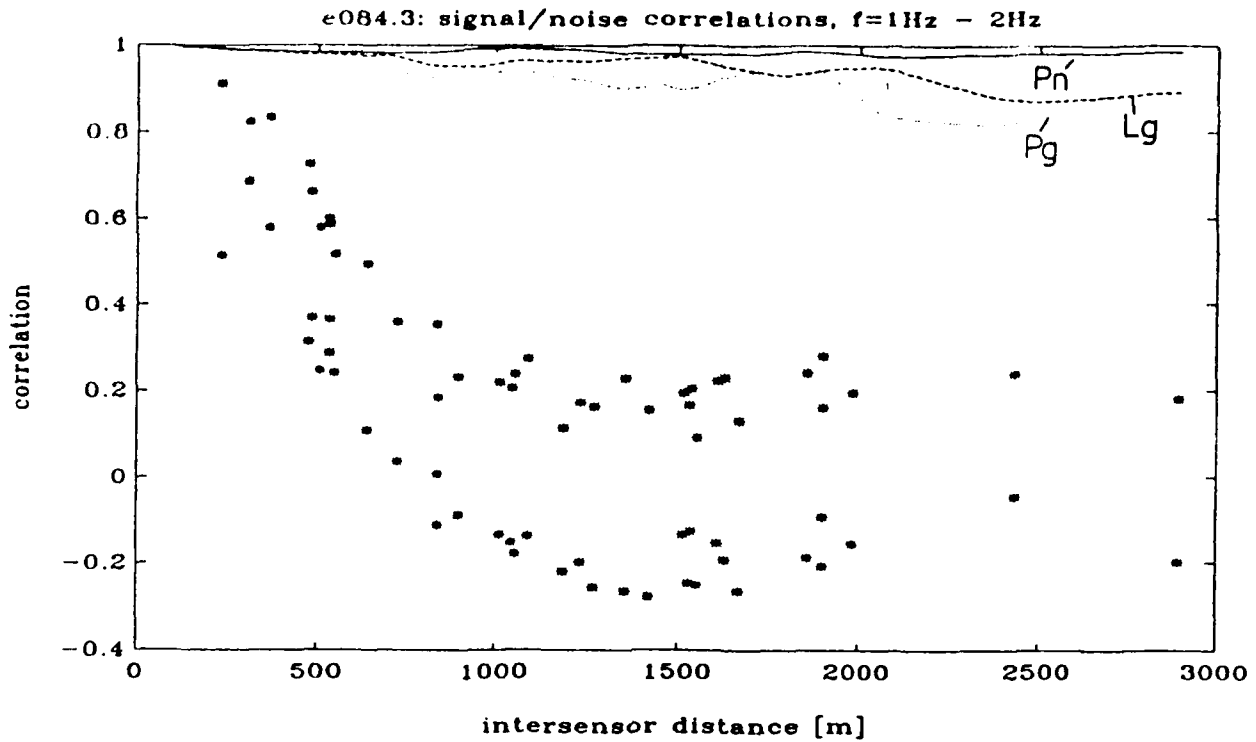
Poland   25. 03. 1989 $\Delta = 354$ km $m_L = 3.8$

Fig. 10 : Signal coherence curves (top: 1 Hz - 2 Hz passband, bottom : 2 Hz - 4 Hz passband) for the test-array calculated from data of the Lubin event shown in Fig. 8. The stars represent plus/minus one standard deviation of the preceding noise window.
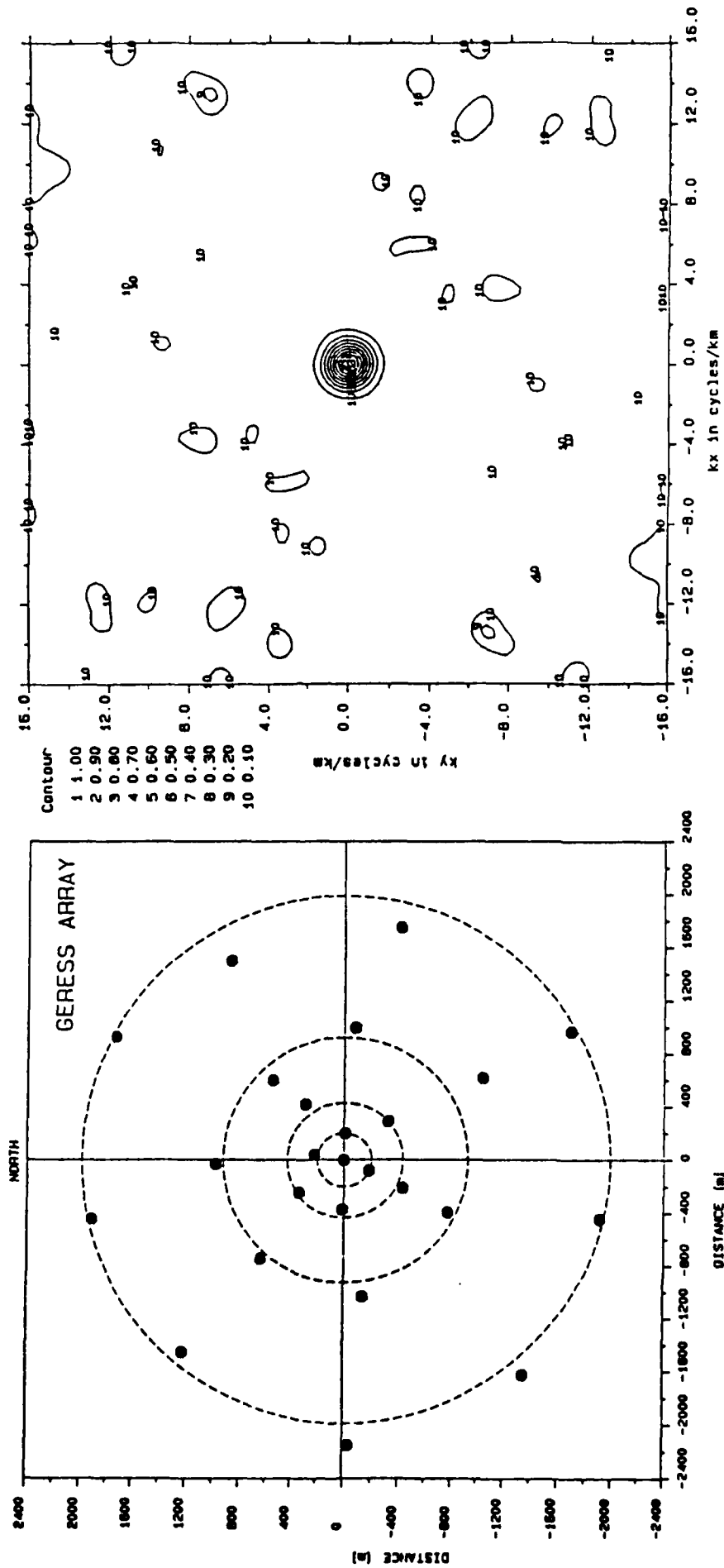
Fig. 11 : Final configuration of the GERESS array including 25 vertical seismometer sites.
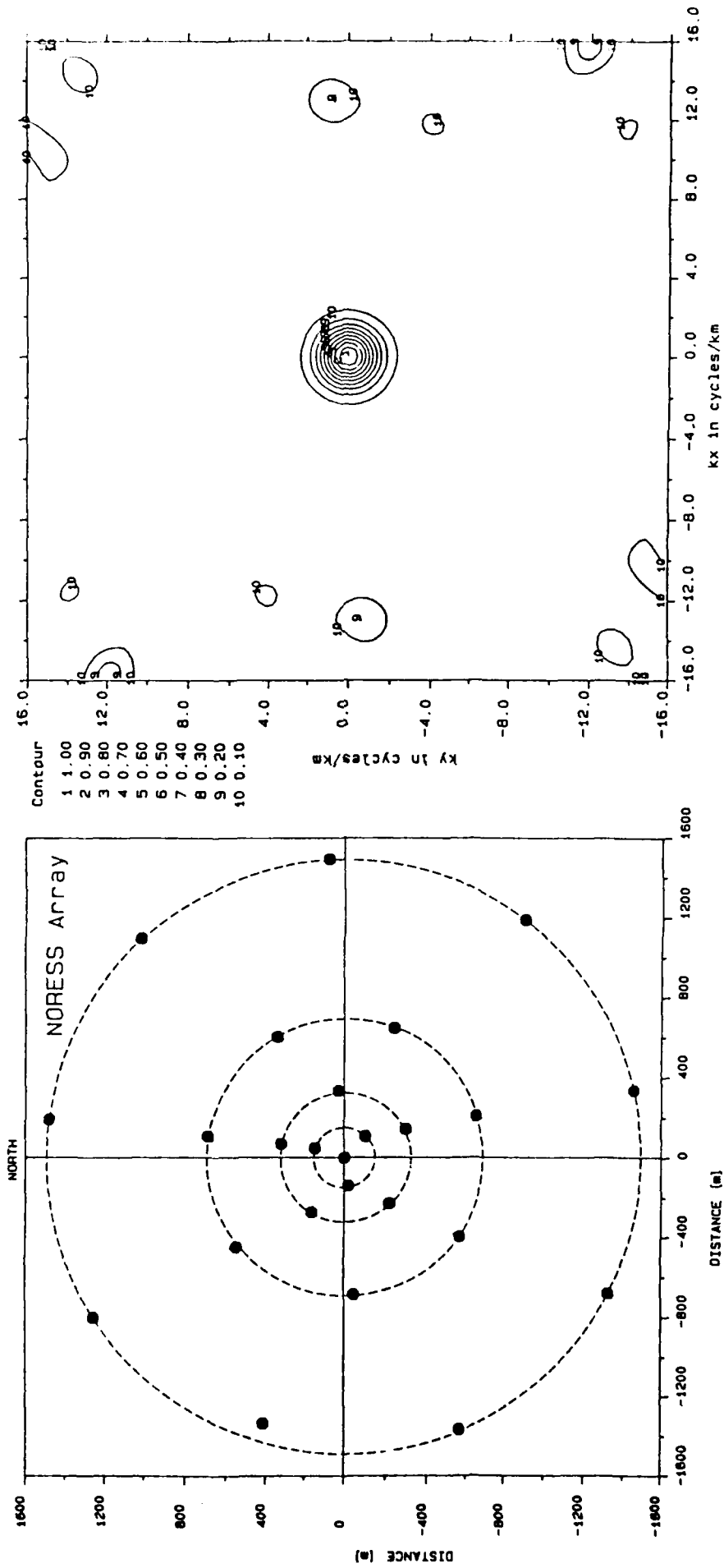
Fig. 12 : NORESS array configuration. On the right the corresponding array response in wavenumber domain is displayed.
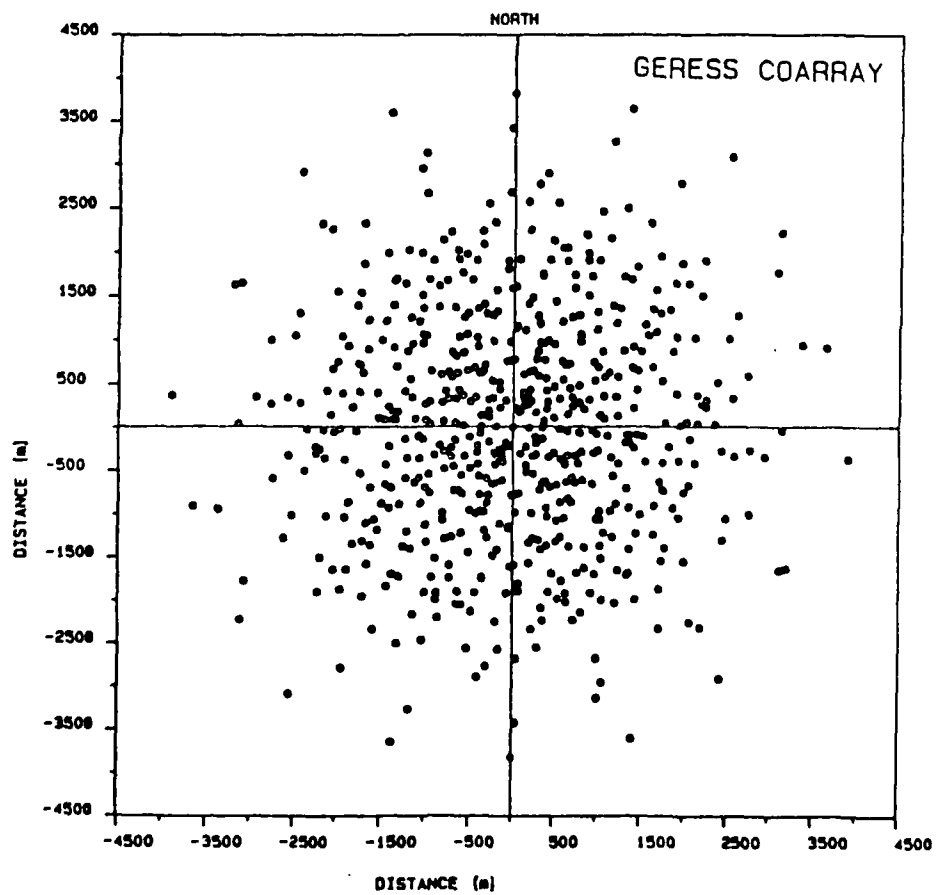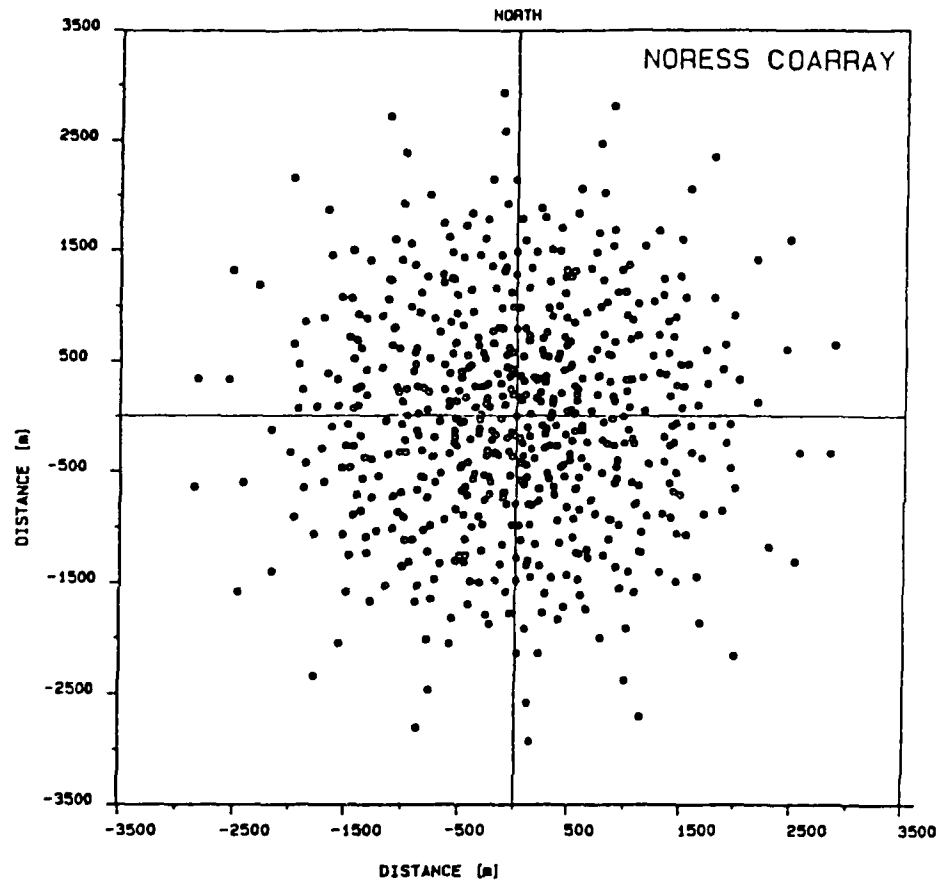
Fig. 13 : Comparison of NORESS (top) and GERESS (bottom) coarray points.
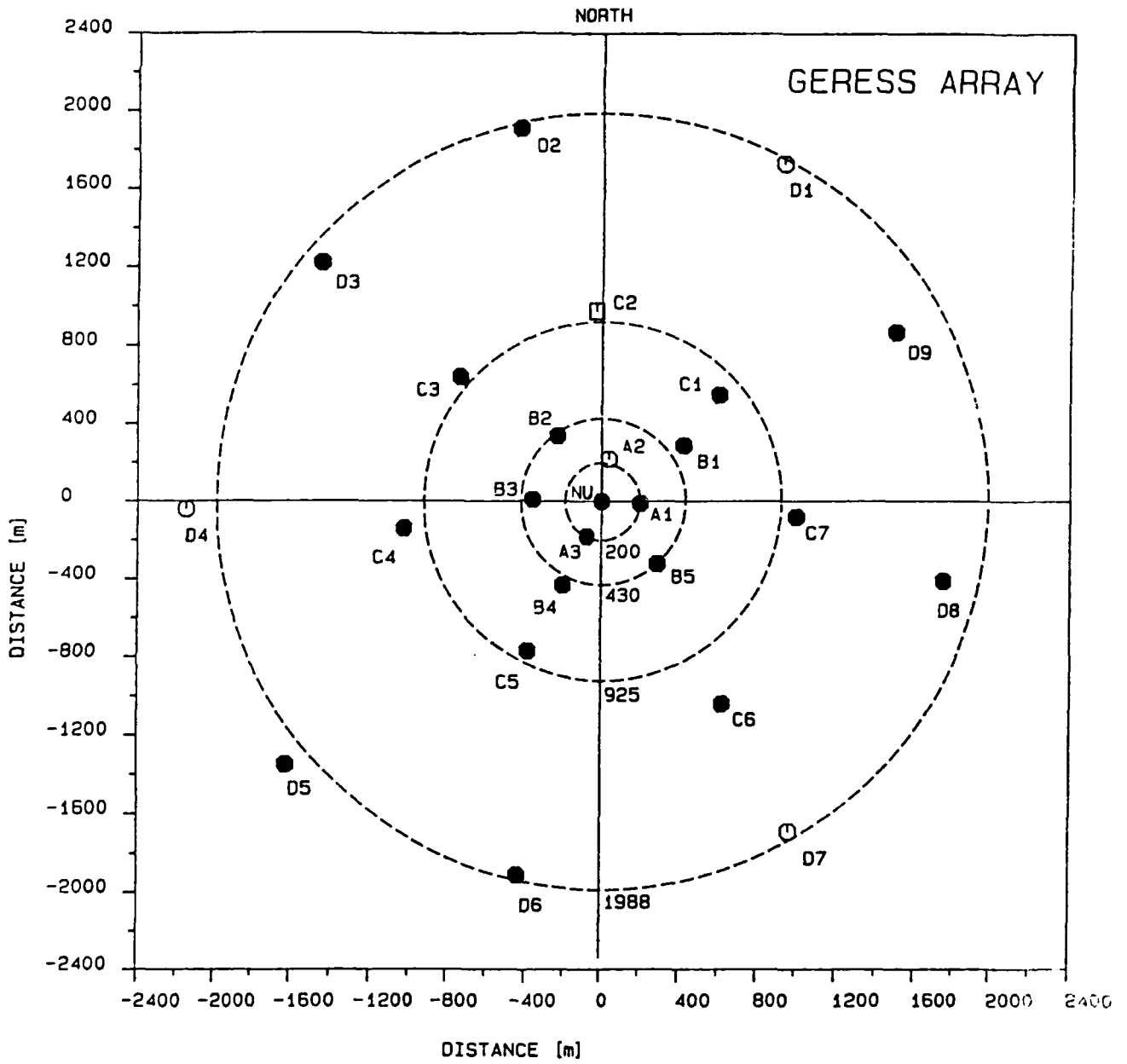
Fig. 14 : The geometry of the GERESS array including station names and instrumentation

II. Module Specifications and Hardware Components
developed for the GERESS Test-Array.

1. Functional Requirements

To get an reliable estimate of the capability of the planned array, the noise and signal coherence had to be determined over short term and seasonal changes. This resulted in a projected measurement time of about half a year and a measurement area covering the whole aperture of the planned array.

The calculation of signal and noise coherency in dependence of station distance requires a long term timing accuracy of 1 msec between all stations.

So the overall design requirements for the test array installation were :

- 9 stations distributed over the array aperture resulting in station distances between 300m - 2200 m from the central station

- timing accuracy of 1 msec in the whole network

- sampling rate of 100 Hz

- digital data acquisition with high dynamic range and resolution

- measurement time of half a year - mostly in winter 1988/89

- unattended operation of the remote stations for at least one week because of the limited personnel

- event oriented data storage because of the huge amount of raw data produced in high frequency mode

2. Available equipment

At date of the planned test installation, the only digital field measurement units available off shelf were Geotech's PDAS 100, in it's first production run with rudimentary software, however. They fulfilled the requirements of high precision digital data acquisition, but failed in some other important requirements listed above:

- Timing accuracy of free running units was excellent on a short term base, but unacceptably bad for a long term installation.

- Power consumption would require a change of the battery pack every few days.

- The limited memory and lack of a coincidence detector to avoid false alarms would even in an event triggered mode require data transfer to a laptop on-site every few hours.

The test array was to be installed in a forest area with few roads, the operators were expected to be quite busy with processing and archiving data in the central station at the SUN workstation. So any solution requiring frequent on-site inspections was impractical. Instead power supply, timing synchronization, coincidence trigger and data transfer from PDAS to PC had to be performed from the central station. Fortunately the array site allowed for long-line cable installation and the electronic laboratory of the Institute of Geophysics had to build the necessary interface modules.

3. System Configuration.

The overall technical design of the test array is shown in Fig. 15 :

Eight remote units, consisting of one S13 and PDAS 100 each, are connected via 4-pair telephone cable with the central station. One pair is for power supply (by 60V DC and DC/DC conversion to 12V), another for 1 PPS timing signals. The remaining pairs form a short haul modem connection between PDAS and PC (RD and TD only, software handshake), while the hardware handshake (DCD, DTR) is used for trigger in/out.

The central unit was connected to a three-component set of S-13 seismometers. It evaluates the trigger-in from all stations by its digital IO facility and provides the coincidence trigger for the whole array (trigger-out). Additionally a DCF-receiver provides the 1 PPS signals for the whole array. Data transfer is done by connection of laptop 2 with one remote PDAS via serial link (KERMIT). During this time (.5 MB in approx. 20 min) data acquisition has to be suspended due to the single task architecture of the current software version in PDAS.

Figure 16 is the circuit diagram of the driver card in the central station rack for each remote unit. The key-switch disconnects the power supply and initiates a remote boot-up of the PDAS. The BC 177 is the driver for the current loop in the 1 PPS transmission.

Figure 17 shows the pulse generator for the 1 PPS by a monoflop 74121 and amplifiers for each remote unit.

Figure 18 gives details of the connection from PDAS unit 0 (the central unit) and laptop 2 to the remote units via modems 1-8 (type MA-14/MA-18 of Hedin Tex AB, Sweden). Selection of one remote unit for data communications will disable trigger transmission via IC 4001 for this station, so the selection for unattended operation is '0'.

Figure 19 shows the connection box at each remote station. Its purpose is to provide the signals needed by PDAS 1-8 from the connection to the central station via telephone line. Power is supplied by a DC/DC converter, while opto-coupler CNY 17-4 decodes the 1 PPS signal. Hardware handshaking of the modem MA-19 is used for trigger in/out, while IC 4528 and relays K1 and k2 are needed for the remote boot up by disconnection of power in the central station (because of the buffered power supply by the battery pack this would not work otherwise).

4. Experiences

The half-year installation time proved most of the above design criteria. The on-site inspections were reduced to monthly intervals needed only for check of the mechanical installations. Data transmission and power supply worked without difficulty.

Some problems however arose due to the immature software in the PDAS. Without any systematics the clock sometimes confused the 1 PPS resulting in a 1 second time offset. This was seldom however and quite easy to verify and to correct in the data subsequently.

Another problem was the unaccurate timing of the detector. Due to the time windows processed on block by the signal processor of PDAS, detection time was only a rough estimate and dependent on the relative timing of processing blocks to seismic signal in each station. This demanded an unreasonably long time window for the coincidence detector not correlated to signal propagation time in the array any more.

M. Joswig
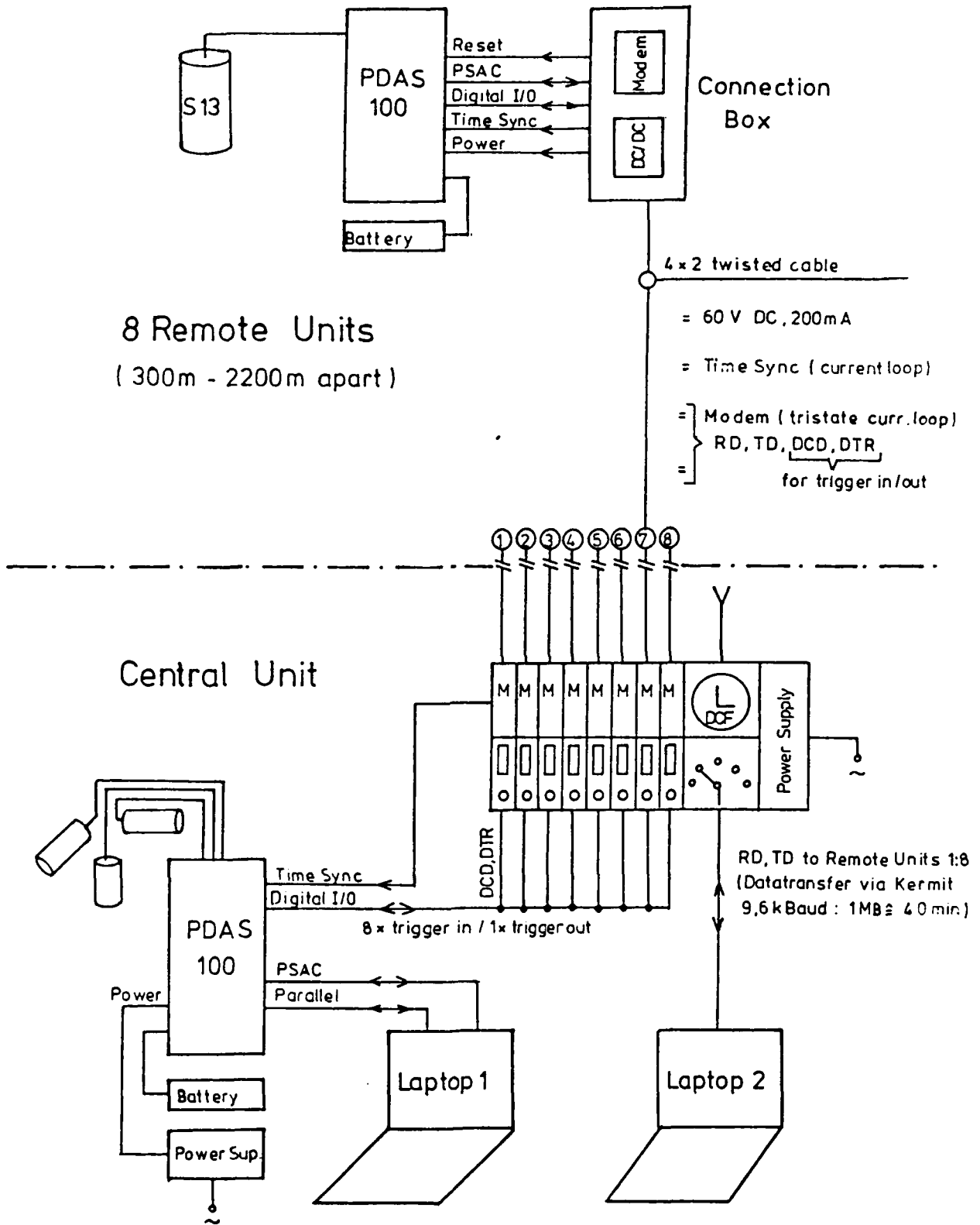
Fig. 15 : Block diagram of GERESS test array

Fig. 16 : Circuit diagram of connection box at remote site

Fig. 17 : Circuit diagram of switch unit PDAS1-8 to laptop 2
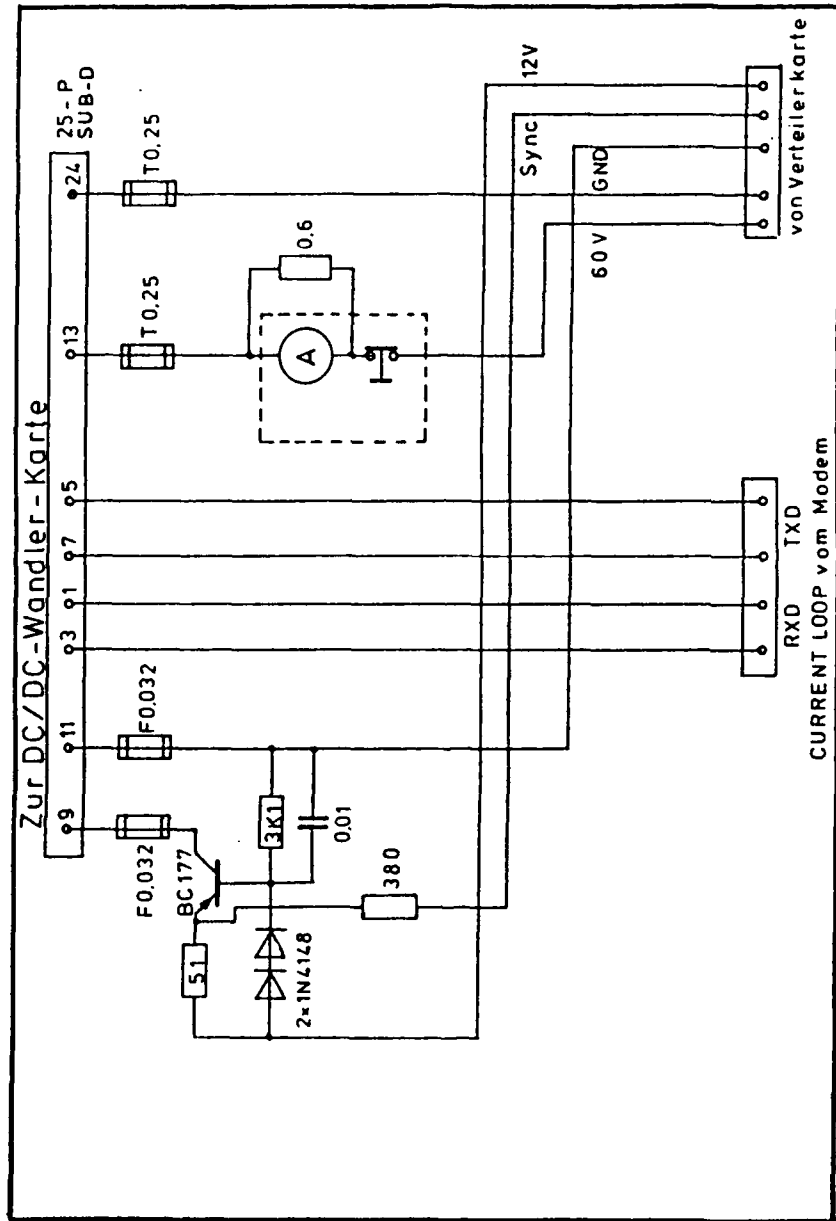
Fig. 18 : Circuit diagram of line driver for 1 PPS timing signal
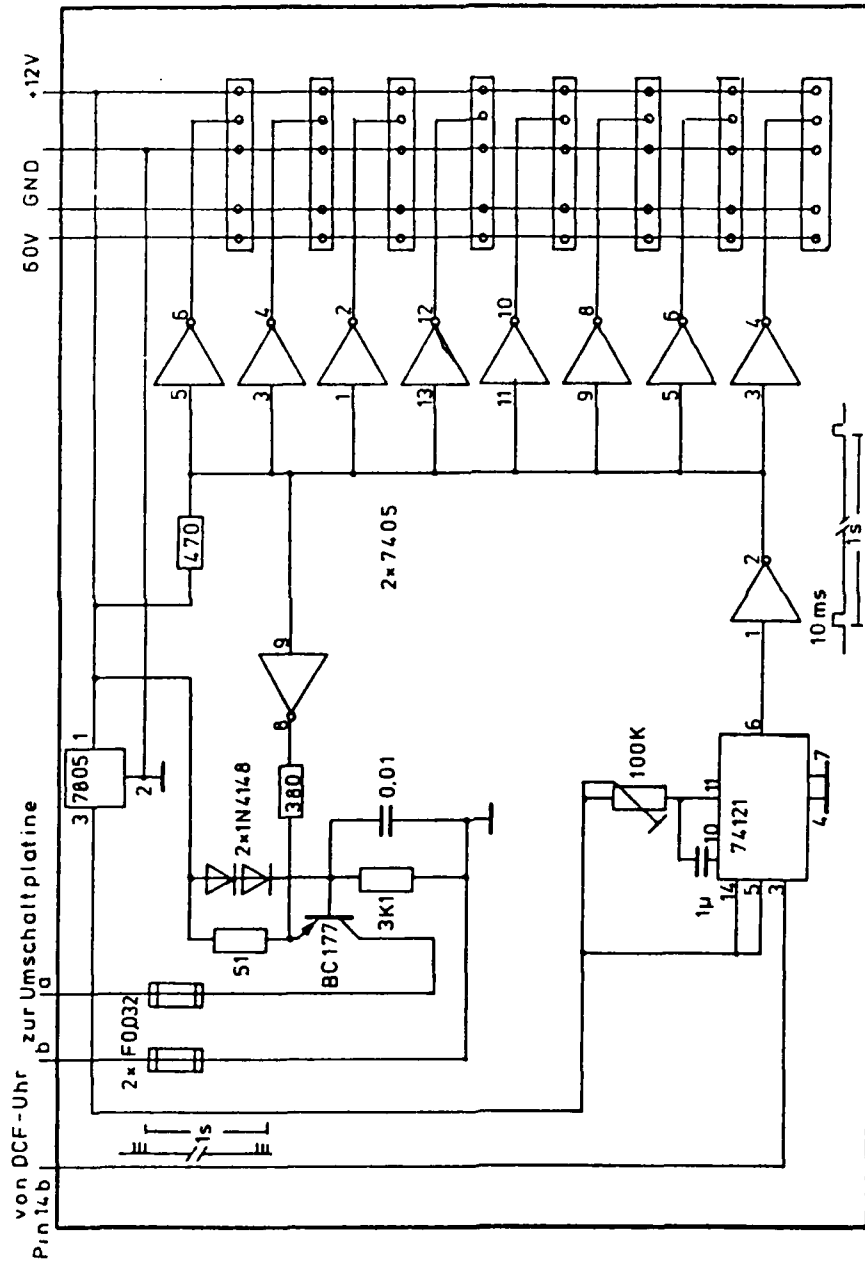
Fig. 19 : Circuit diagram of pulse shaping and buffer amplifiers for 1 PPS

ZENTRALE: Verteilerkarte

13.2.89 | O. Richter

Sheet 2 / 4

III. Event recordings from the Geress test-array

As outlined in chapter II, the data acquisition system principally operated in detection mode. A conventional STA/LTA - detector was implemented on the single PDAS-100 channels and a time window was set in which a minimum number of channels had to trigger.

Using an updating LTA the recording length was variable but generally complete seismograms for regional events from Pn-waves to Lg-waves were recorded.

After inspection of the detection times which were compared with bulletin data, i.e. PDE for teleseismic events and EMSC for regional seismicity, the corresponding waveforms were stored in a data base using CSS 2.8 format.

The operation of the test-array covered a time period from December 8 1988 to April 4 1989. Due to technical problems related to the temporary installation, the actual recording time was only 92 days of the total time period.

Altogether 276 events were recorded and summarized in an event list. 112 events were classified as local within an epicenter distance of 150 km, they originated mostly from quarry blasts in Czechoslovakia and Germany. Additionally 67 teleseismic events (distance greater than 2000 km) were recorded and finally 97 events occurred at regional distances (150 km - 2000 km).

As the planned array is specifically aiming at high-frequency signals particular emphasis was given to the evaluation of these regional events. Table 1 contains a list of nine events which were selected for even azimuthal coverage. The epicenters of these events are shown in Figure 20. We start our discussion with event 1 (Figure 21) originating from Lubin in Poland which was already displayed in Figure 8. In a previous report (Harjes, 1989) it has been mentioned that two mining districts in Poland cause remarkable seismicity, namely the copper mine near Lubin and the coal mining district near Katowicz.

These events exhibit very consistent Pg- and Lg-phases which dominate the seismograms. A clear Pn-onset is often missing in the seismograms from the coal mines and this difference can be attributed to the different geology in the source region.

Seismic waves from event 2 (Figure 22) traveled the shortest distance of 265 km from the epicenter in Austria to the GERESS test-array. With its sharp Pn-phase the event looks explosion-like although it is reported as a shallow earthquake and a close look, indeed, shows a weak starting phase. About 4 sec after the first arrival, we see a clear P*-phase whereas the Pg-phase is almost hidden in the coda. Accordingly, the S-wavetrain starts with the S*-phase and no distinct Sg- or Lg-wave is visible.

Continuing further to the South on our epicenter map, event 3 (Figure 23) shows an earthquake from Hungary with an emergent Pn-phase followed by a long coda. No clear later arrivals can be recognized although the Lg-amplitudes are easily detected.

The following two events (no 4 and no 5 from table 1) which are plotted in Figure 24 and Figure 25 originate from the same source region at the Adriatic coast of Jugoslavia. They set an example for the differences in phase amplitudes which can exist for very close epicenters. While event 4 contains a clear Pg-phase but almost no Lg-phase, event 5 shows just the opposite. In addition, the Sn-phase is also very different for both earthquakes> event 4 exhibits two distinct S-phases, the first of which is certainly the Sn-phase, while the second could be interpreted as an S*-phase. Consequently, these two earthquakes would constitute a challenging task for an automated event processor.

The next three events (nos 6 - 8), plotted in Figures 26 - 28, come from southeastern azimuths and the seismic waves travel Alpine wave paths. The amount of high frequencies in all three recordings is surprising, Pn- and Sn- waves are dominant, both phases are followed by a long coda. Unfortunately the recording window for two of these events was too short to discuss the Lg-wave amplitudes. For event 6, originating in Northern Italy, the data quality is poor and only three traces are recorded for the expected arrival time for Lg-waves but there appears to be no signal. The situation is similar to the earlier discussed events from Jugoslavia where Lg-waves appear and disappear within small epicenter differences. The same observation holds for the Pg-wave. From a clear onset in event 7 (Figure 27) the Pg-amplitude decreases to the Pn-coda level for event 8 (Figure 28).

The last regional earthquake from table 1 is plotted in Figure 29 (event 9). Waves from this event strike the test-array from a northwestern azimuth and the general picture of the seismogram looks like event 1 which had a bearing to the northeast. The crustal phases Pg and Lg dominate the seismogram, the Pn-phase shows very small amplitudes and Sn is not discernible.

In concluding the description of regional seismograms recorded at the test-array, two limitations should be mentioned: firstly, the source mechanism and size of the events will also influence the relative excitation of different wave types and secondly, the characterization of regional seismograms by the few traditional phases can only be regarded as a first order approximation.

Nevertheless, the differences in regional phases can also be demonstrated in the frequency domain. In Figures 30 - 32 a power spectrum of those phases together with the background noise is plotted. Figure 30 shows the main difference between an event from northern azimuth (no 1, Poland) and an earthquake from southwestern azimuth (no 8, Switzerland). In both cases the sampling rate was 100 Hz, i.e. the antialiasing filter cuts the information at 40 Hz. Whereas the spectral amplitudes of the signal phases for the Polish event stay above the noise spectrum for frequencies below 20 Hz with an optimum SNR around 2 - 3 Hz, the Swiss earthquake shows excellent SNR's out to 40 Hz.

It would certainly have been interesting to record even higher frequencies. This unusual frequency behaviour is confirmed by the second Swiss earthquake (no 7 in Figure 32) which strikes the test-array from roughly the same bearing. Due to the lower sampling rate of 50 Hz the antialiasing filter acts already at 20 Hz.

Events from southeastern azimuths (Figure 31, events no 3 and no 4) show a rather steep spectral slope comparable to the Polish event but in contrast to that event the Pn - phase of the Hungarian and Yugoslavian earthquake exhibit the highest frequencies.

Regarding the high frequencies which are a common feature of regional events at distancies below 1000 km, a sampling rate of 40 Hz - as planned for the final array design - is to be seen as a minimum requirement. Higher sampling rates would be desirable and the one high-frequency three-component seismometer which is planned to sample at 120 Hz will become of great importance.

At distances of 1000 km and more the waveforms from earthquakes in Greece and Turkey as well as from southern Italy and northern Africa are very complex, no significant signal energy can be recognized above 10 Hz. This observation is in accordance with earlier results from the site survey.

For the same set of regional events the location capabilities of the test-array were investigated. As has been shown earlier (compare Figure 10), the signal correlation proved to be excellent over the aperture of the test-array. On the other hand, a conventional narrow-band wavenumber analysis resulted in large variances for the azimuth estimates depending on the passband of the frequency prefilter. Figure 33 shows the k-analysis for the Polish event (no 1) for four different frequencies. The estimated bearing fluctuates from 34 degrees at 1 Hz to 18 degrees at 4 Hz. In this situation a new method of direction estimation of wideband signals (Nawab et al, 1985) gave excellent results. The method uses the zero-delay covariances of the complex analytic representation of the seismometer outputs to estimate the wavenumber spectrum. The power along each radial direction in this wavenumber spectrum is proportional to the temporal power spectrum of plane wave sources in that direction. Figure 34 gives the wavenumber plots for the Pn phase of 6 events from table 1. The estimated bearings match the theoretical values given in table 1 quite well. If one takes into account that the geometry of the test-array was far from optimal, the location capabilities of the final GERESS array should allow an independent evaluation of the seismicity in Central Europe. Locations derived from GERESS data can be used as starting solutions in a location procedure including single stations from a European network.

References.

Nawab, S.H., F.U. Dowla and R.T. Lacoss (1985). Direction determination of wideband signals. IEEE Trans. ASSP-33, 1114-1122.

region	date	origin time	lat.	lon.	Δ/km	az.
1. Poland	25.03.1989	12:46:40.3	51.62°N	16.11°E	354	28°
2. Austria	11.02.1989	02:46:12.2	47.97°N	17.03°E	265	110°
3. Hungary	27.01.1989	03:55:05.6	47.04°N	16.95°E	315	128°
4. Yugoslavia	16.12.1988	11:35:52.3	44.72°N	15.04°E	470	167°
5. Yugoslavia	13.02.1989	00:35:13.0	44.79°N	14.69°E	457	170°
6. Northern Italy	25.12.1988	18:27:36.1	44.97°N	9.05°E	558	221°
7. Switzerland	07.01.1989	02:29:42.4	46.36°N	7.49°E	543	242°
8. Switzerland	02.04.1989	06:59:00.6	47.19°N	9.01°E	390	244°
9. GDR	13.03.1989	13:02:18.2	50.74°N	9.84°E	349	309°

Table 1 :   List of regional events recorded
with GERESS test-array
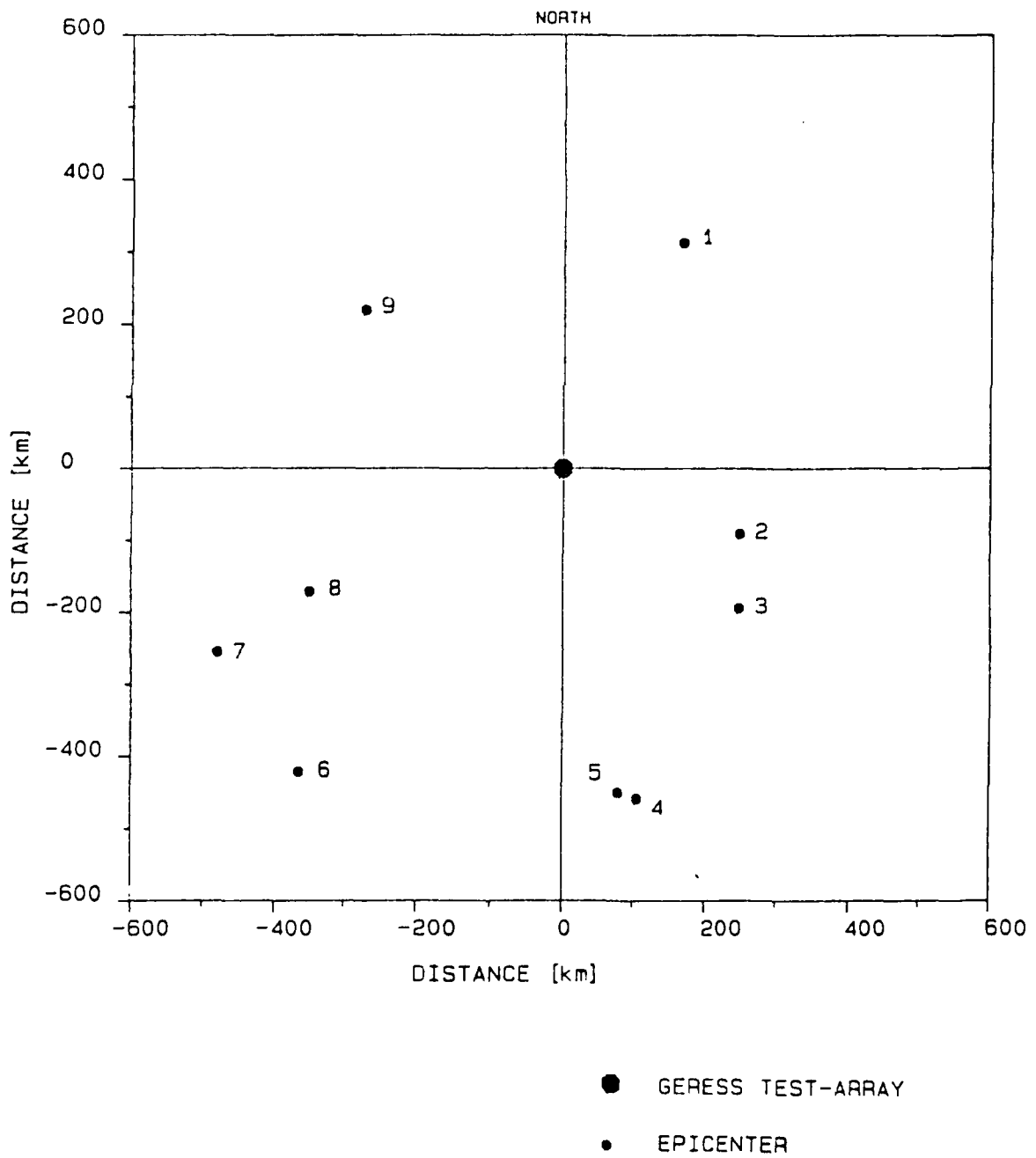
Fig. 20 :   Epicenter map of regional events recorded with GERESS test-array
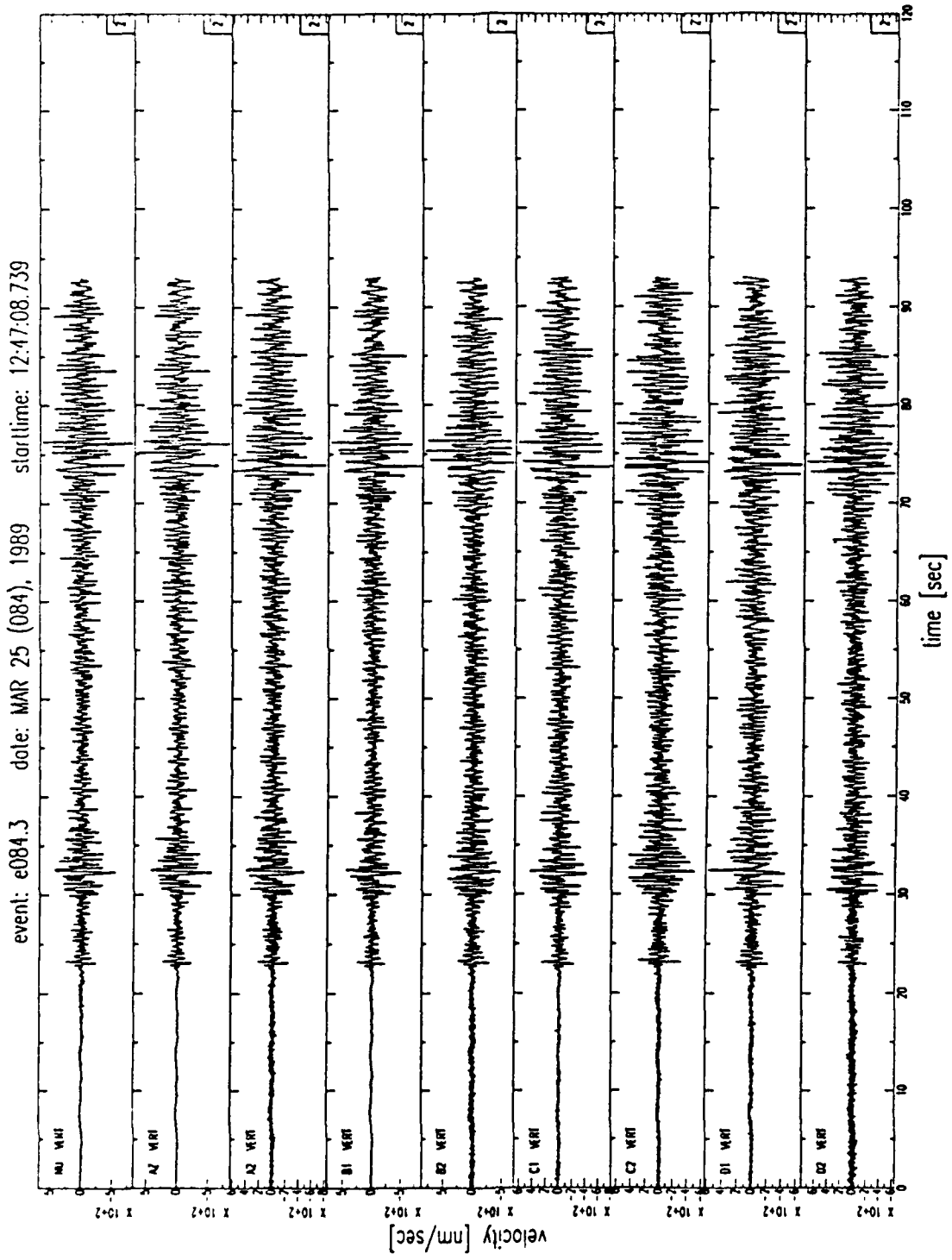
Fig. 21 :   Event : Poland 03/25/1989 12:46:40.3
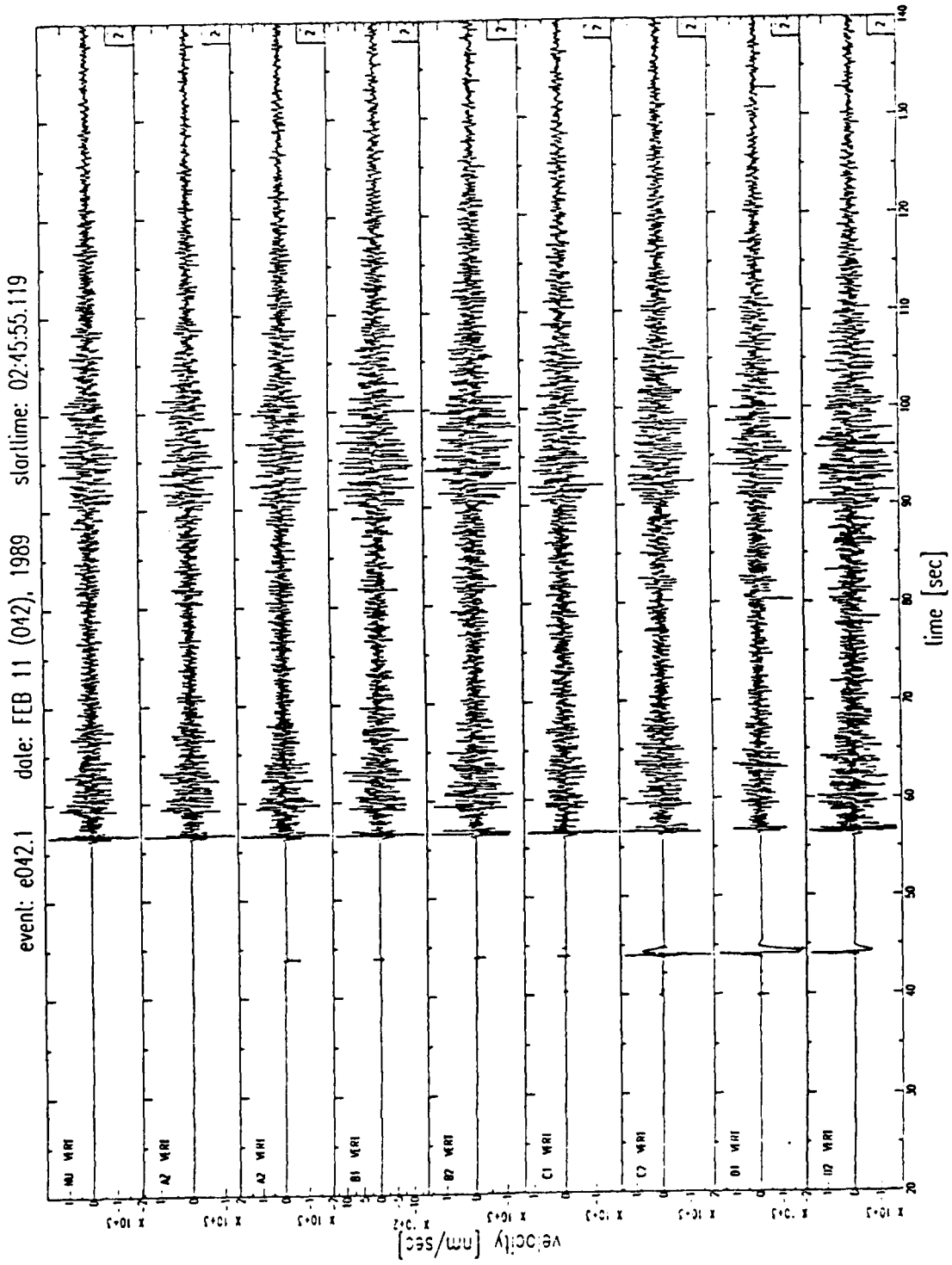
Fig. 22 :   Event 2 : Austria 02/11/1989 02:46:12.2
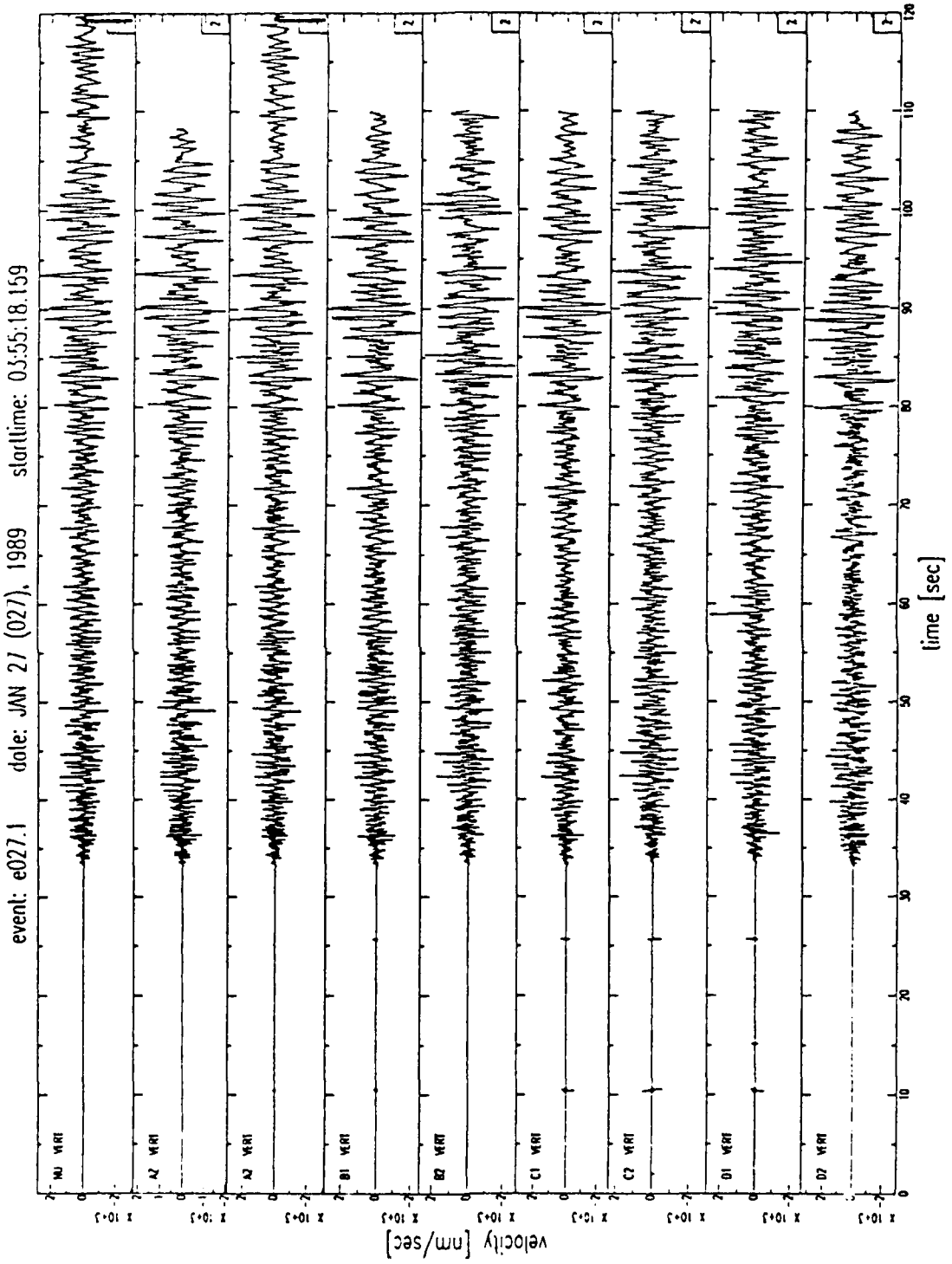
Fig. 23 : Event 2 : Hungary 01/27/1989 03:55:05.6
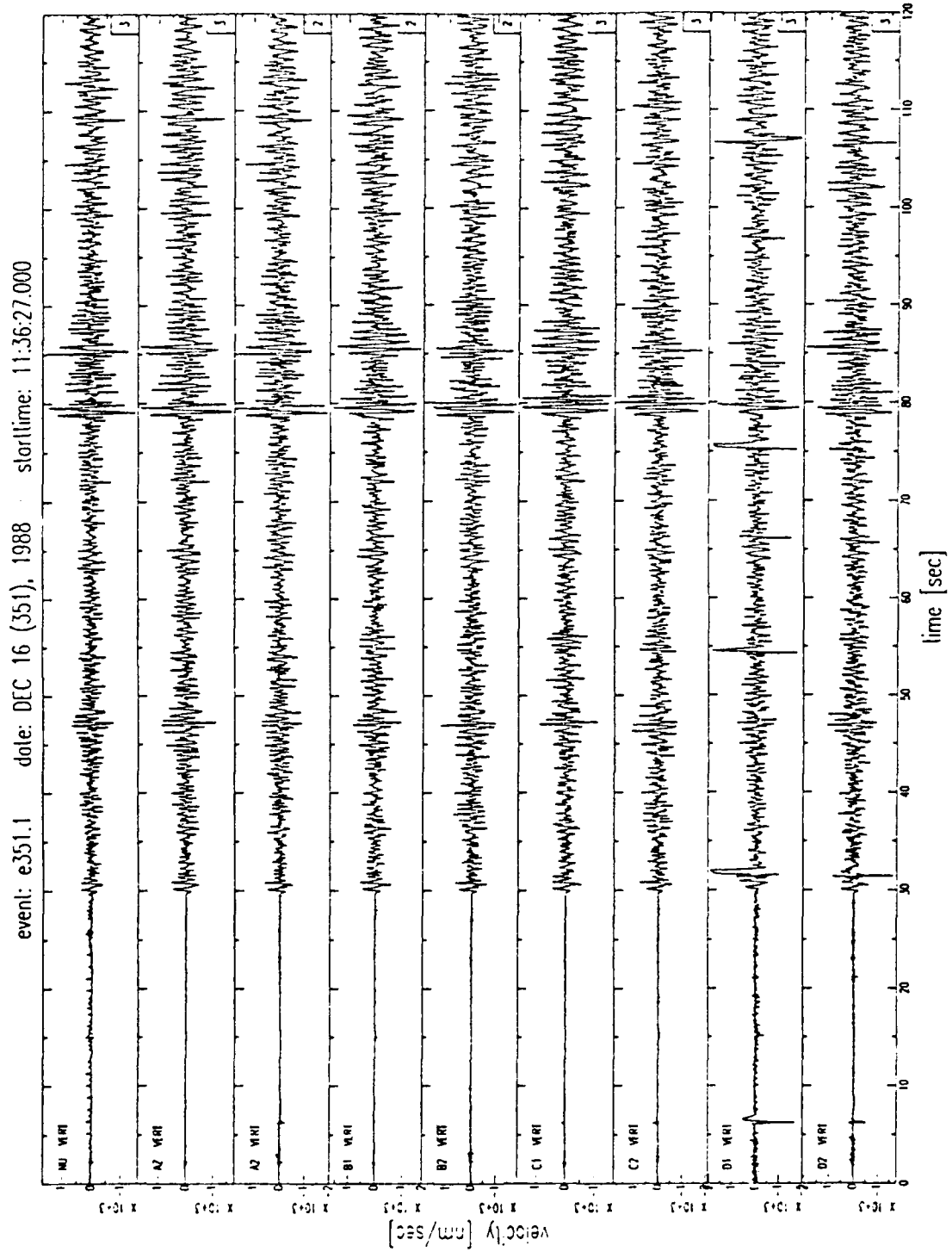
Fig. 24 :   Event 4 : Yugoslawia 12/16/1988 11:35:52.3
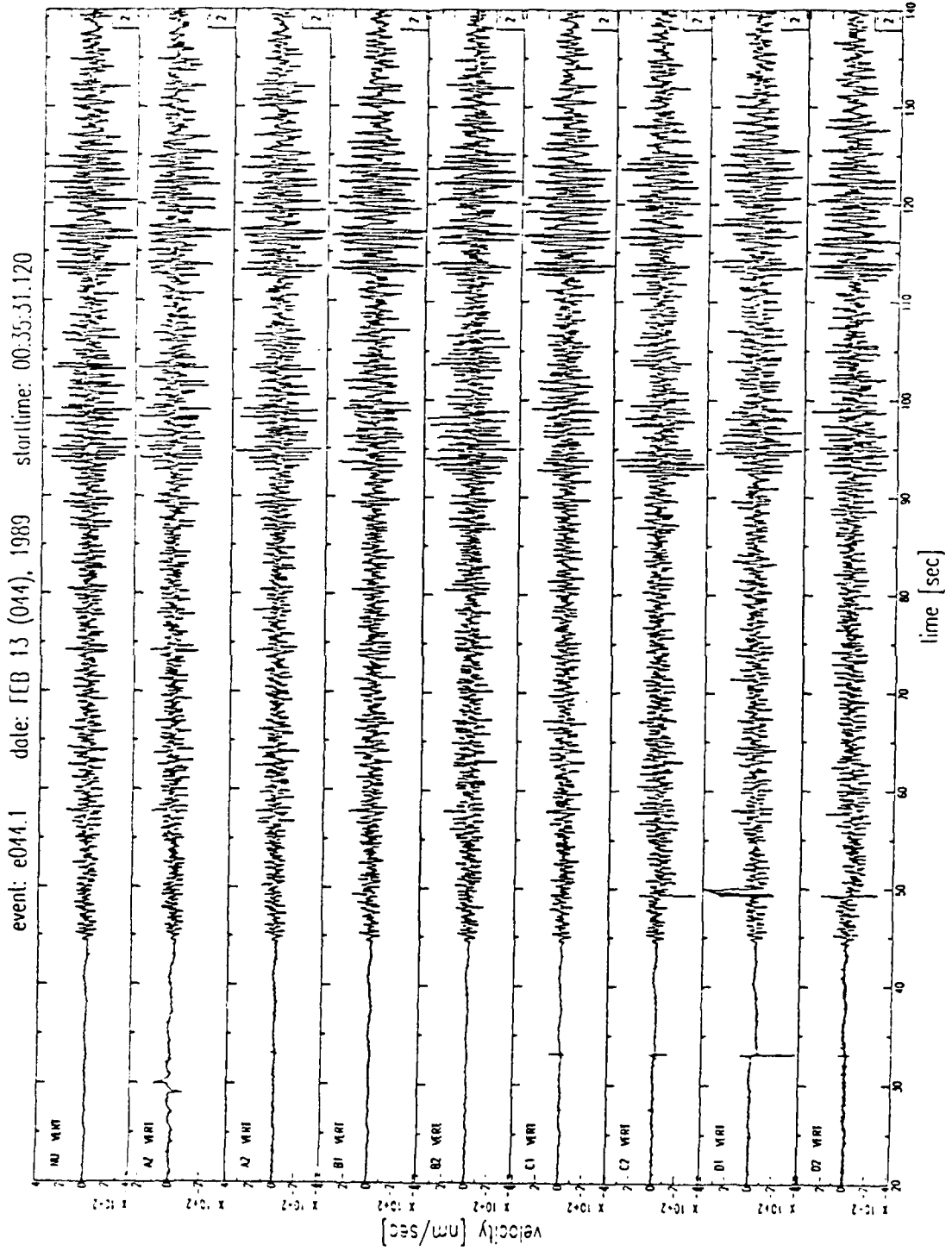
Fig. 25 : Event 5 : Yugoslavia 02/13/1989 00:35:13.0
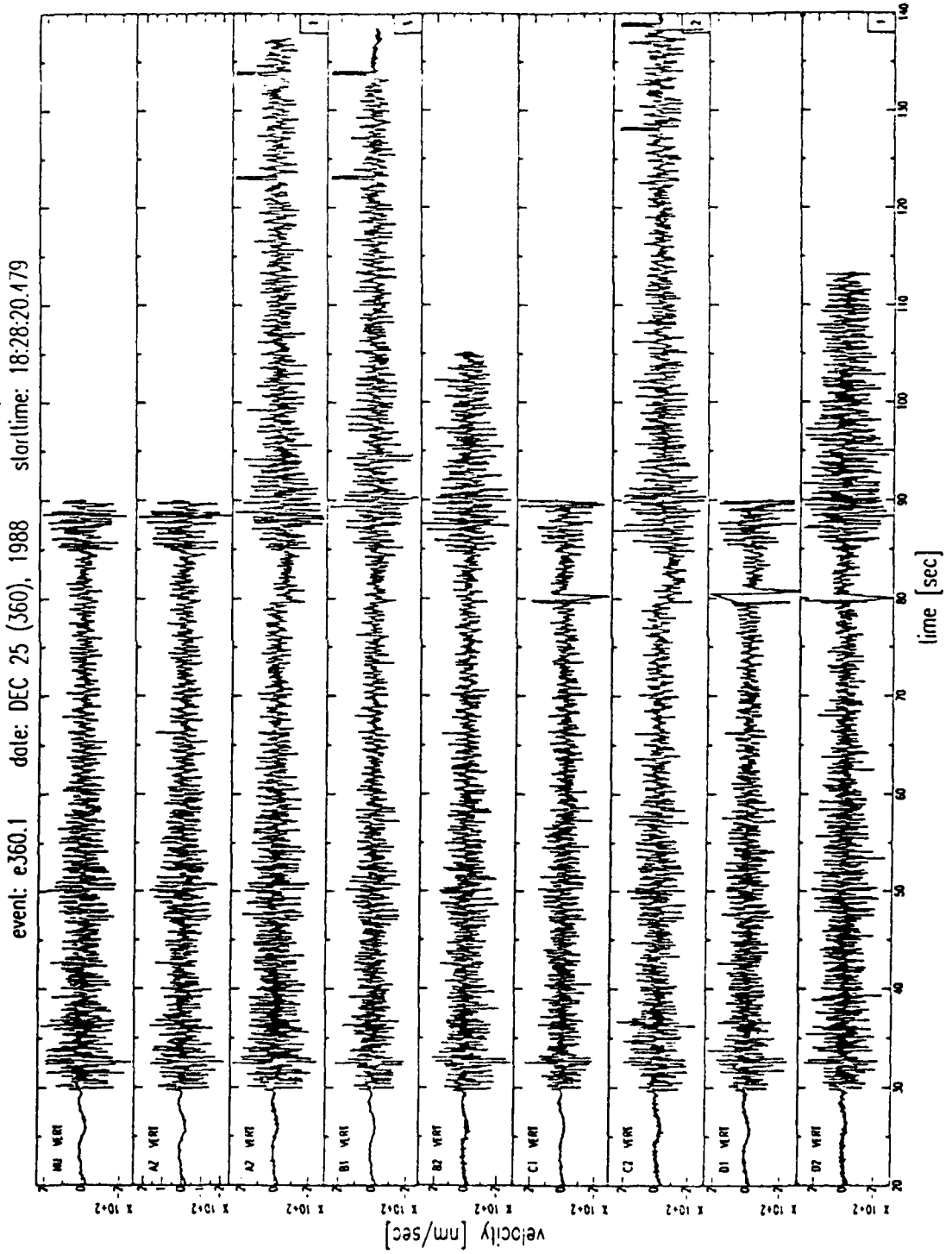
Fig. 26 :   Event 6 : Northern Italy   12/25/1988   18:27:36.1
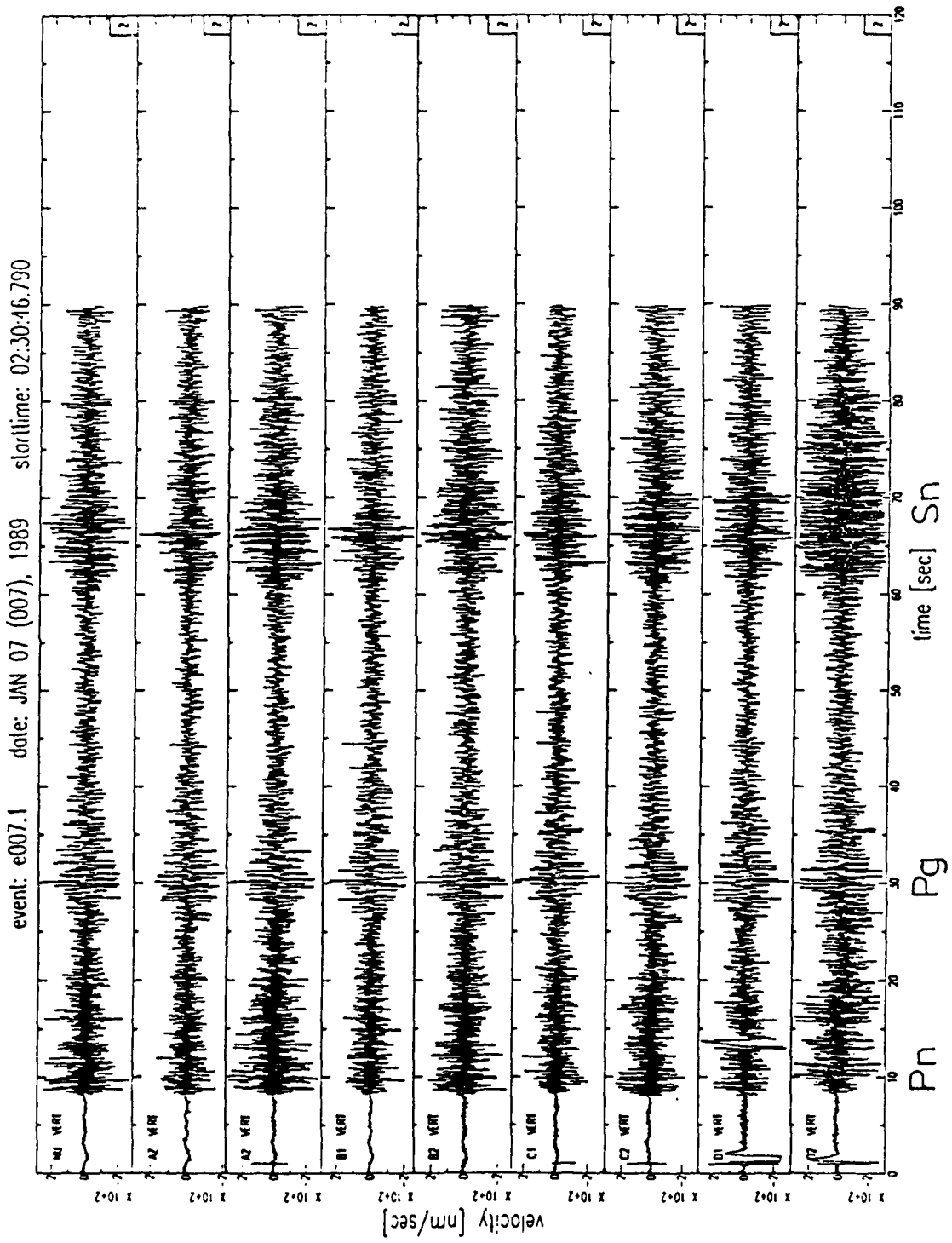
Fig. 27 :   Event 8 : Switzerland 04/02/1989 06:59:00.1
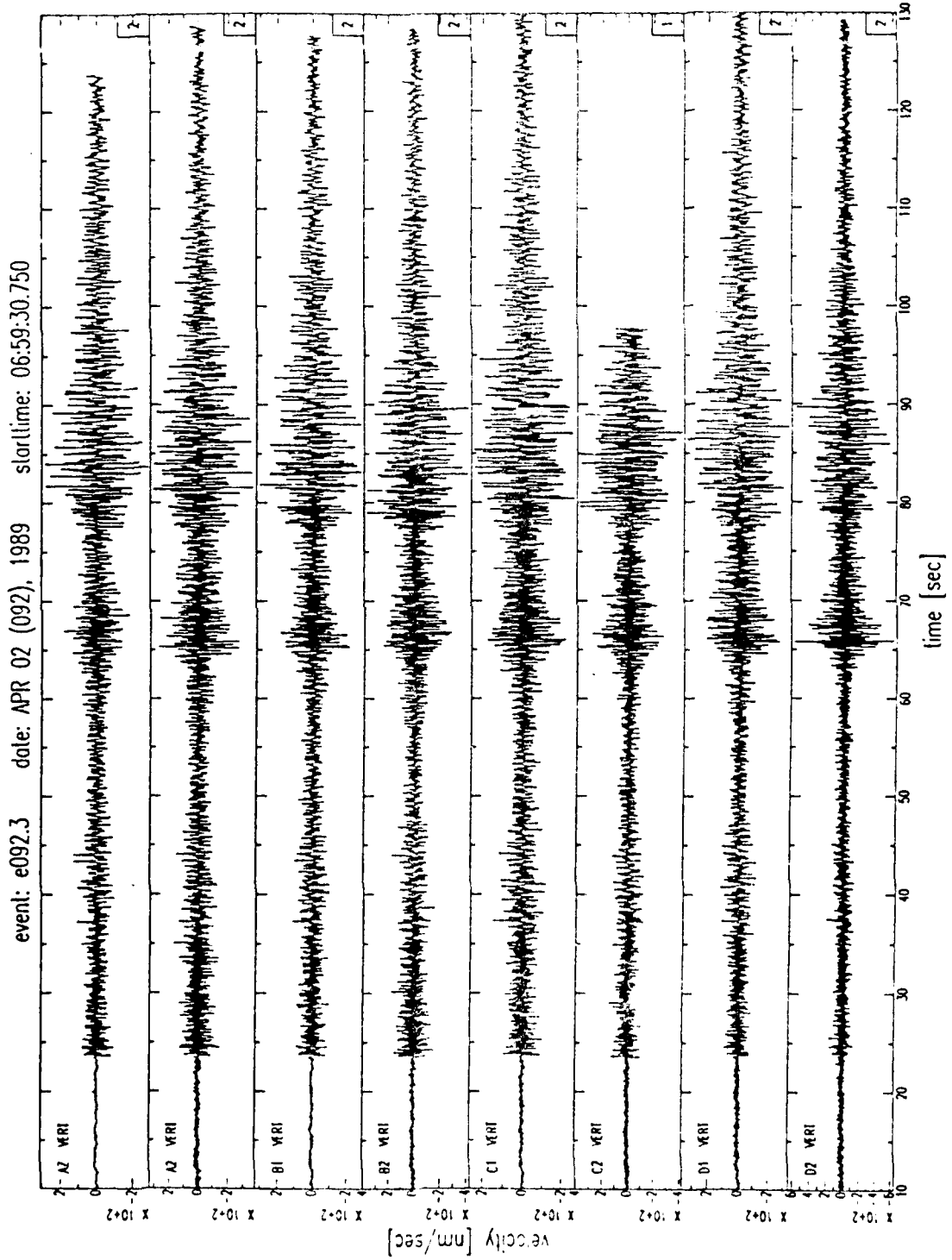
Fig. 28 :   Event 7 : Switzerland 01/07/1989 02:29:42.4
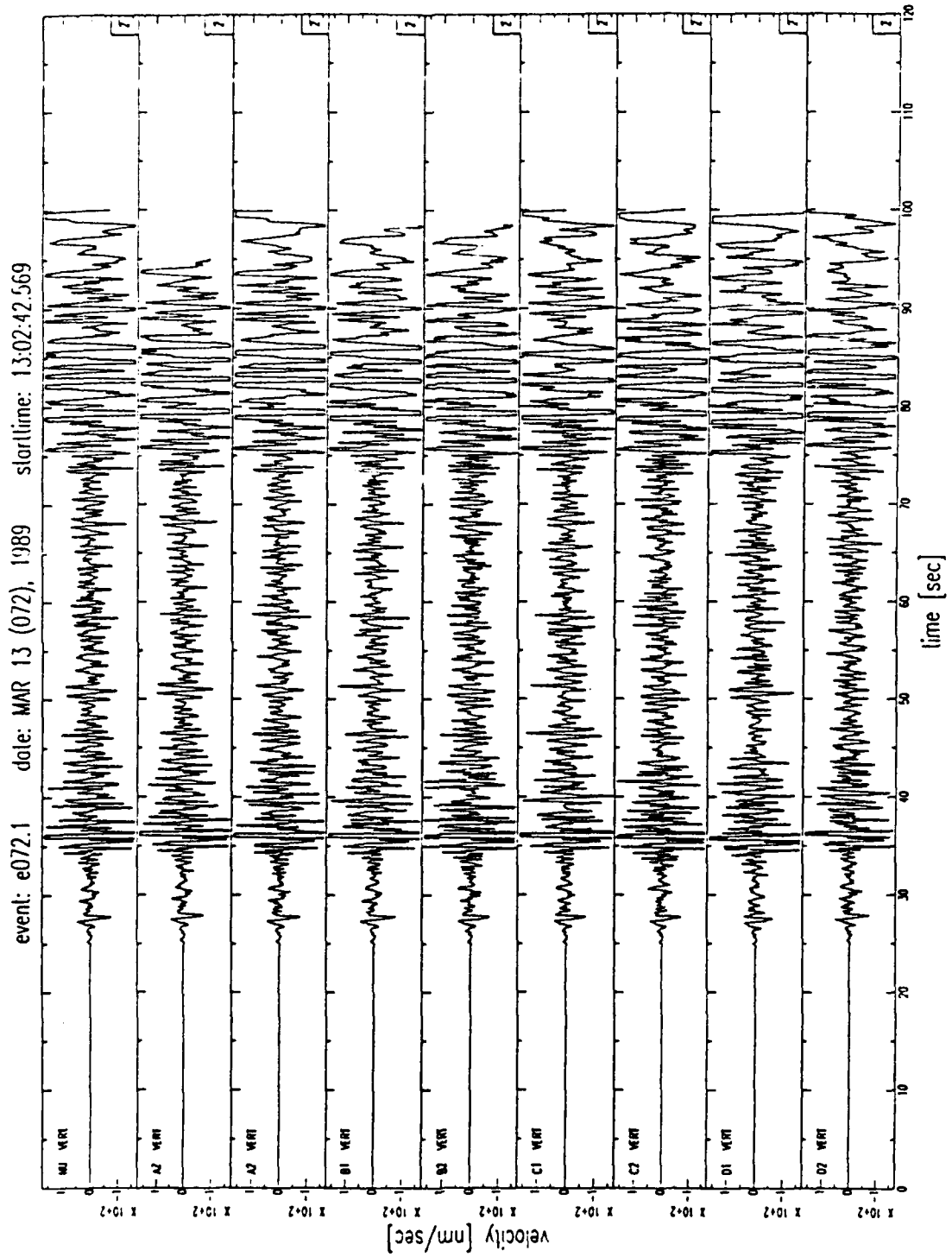
Fig. 29 :   Event 9 : GDR 03/13/1989 13:02:18.2
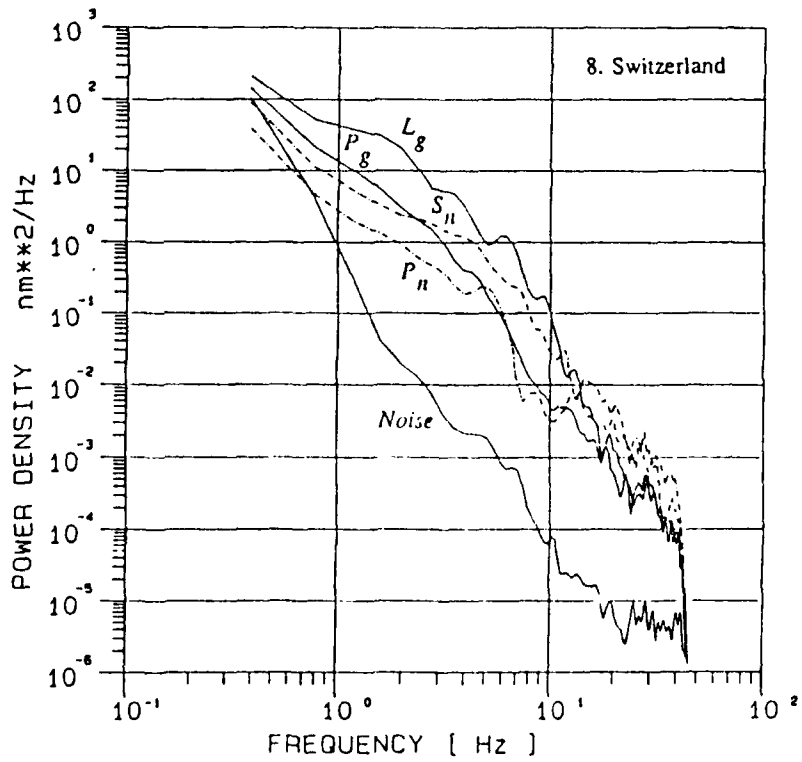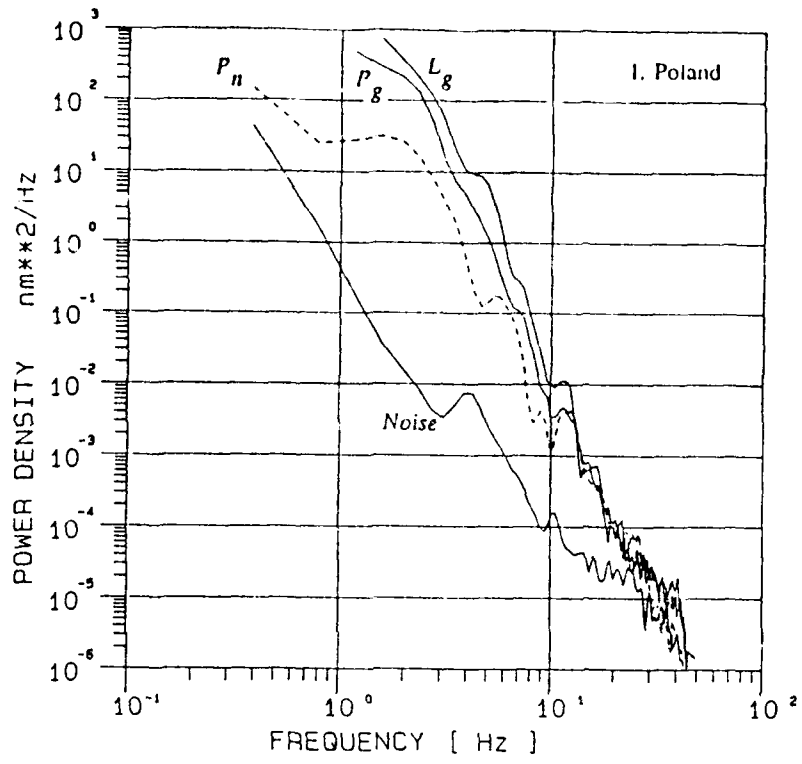
Fig. 30 :   Displacement power spectra of events no 1 and no 8 from Table 1.
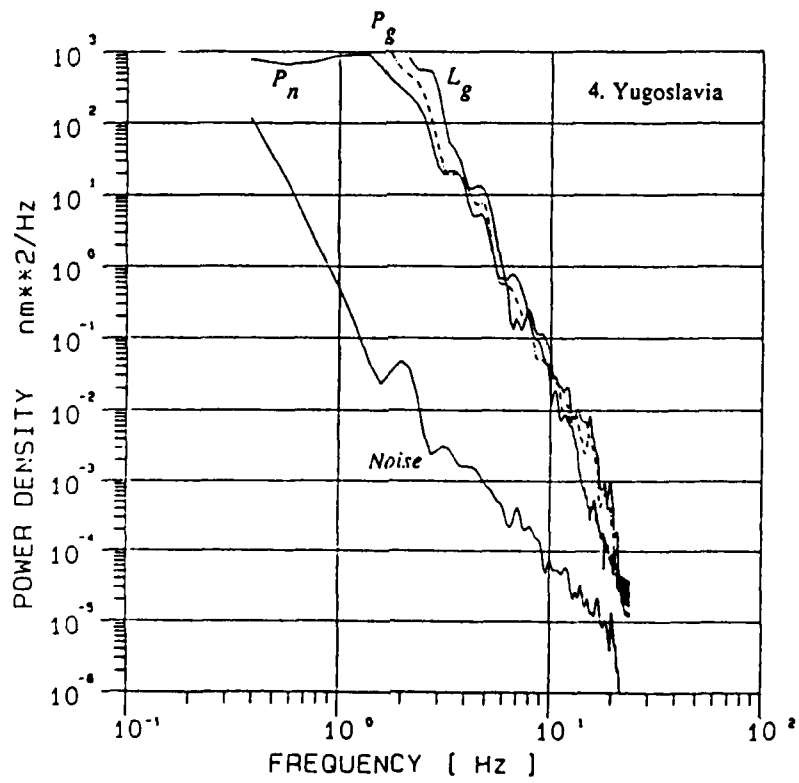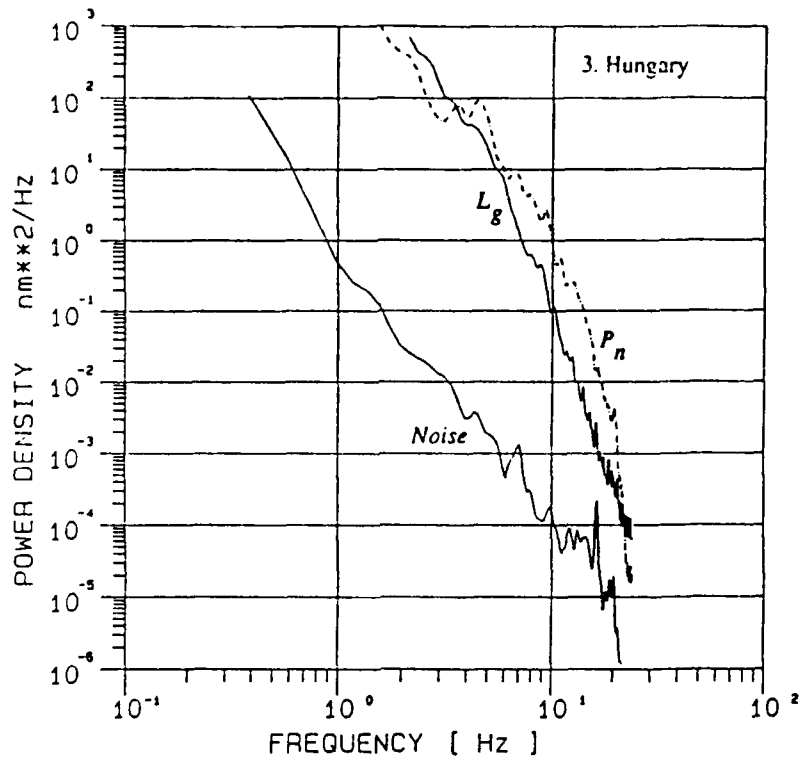
Fig. 31 :   Displacement power spectra of events no 3 and no 4 from Table 1.
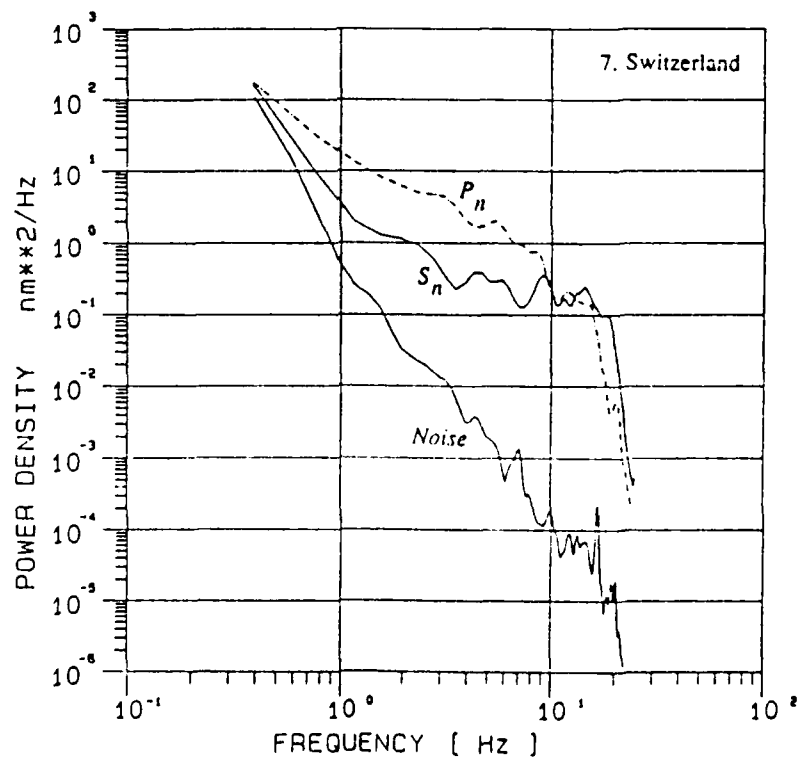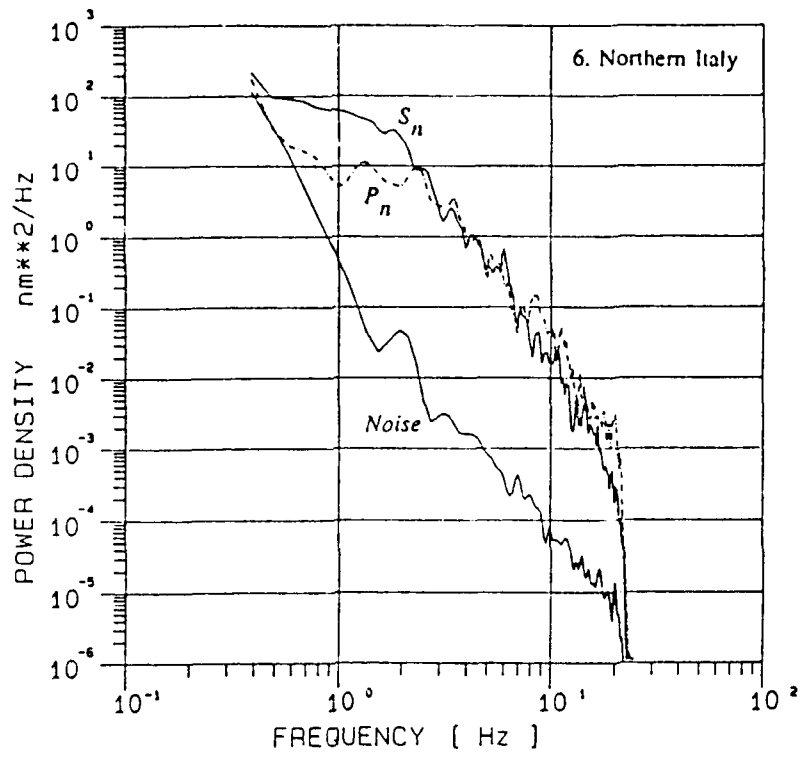
Fig. 32 : Displacement power spectra of events no 6 and no 7 from Table 1.

March 25, 1989 12:47 Pn (22-25 s)
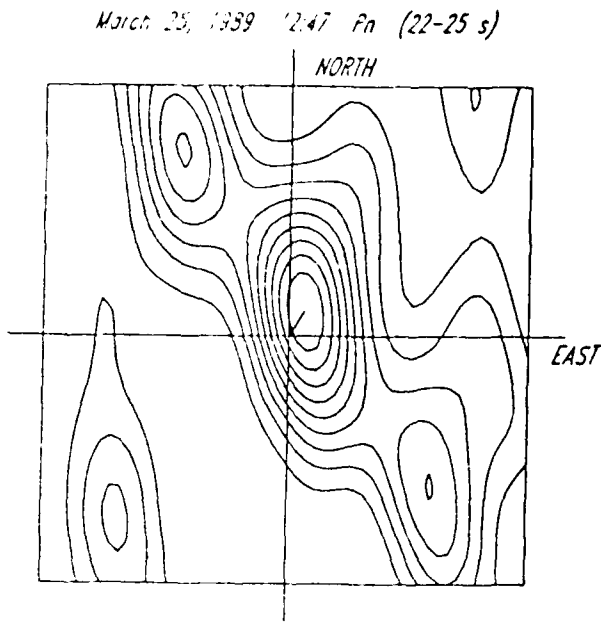
NBFK – single window

Estimated bearing: 33.717

Estimated velocity: 8.1239

Analysis frequency: 1.000

March 25, 1989 12:47 Pn (22-25 s)
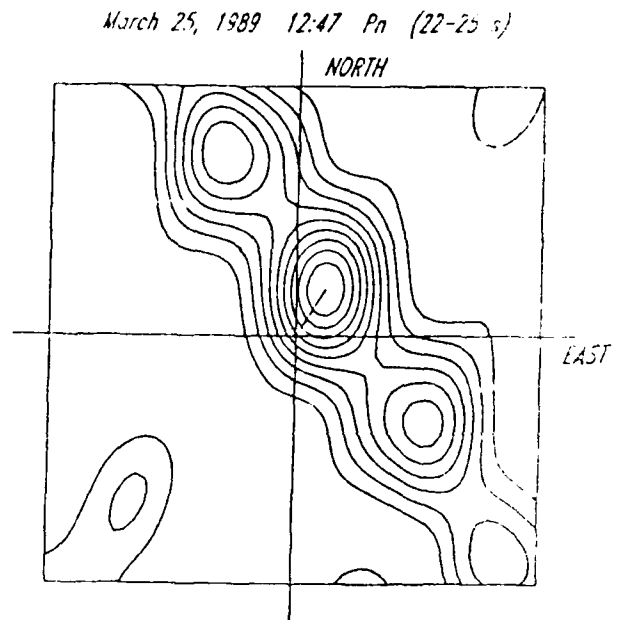
NBFK – single window

Estimated bearing: 31.640

Estimated velocity: 8.9782

Analysis frequency: 2.000

March 25, 1989 12:47 Pn (22-25 s)
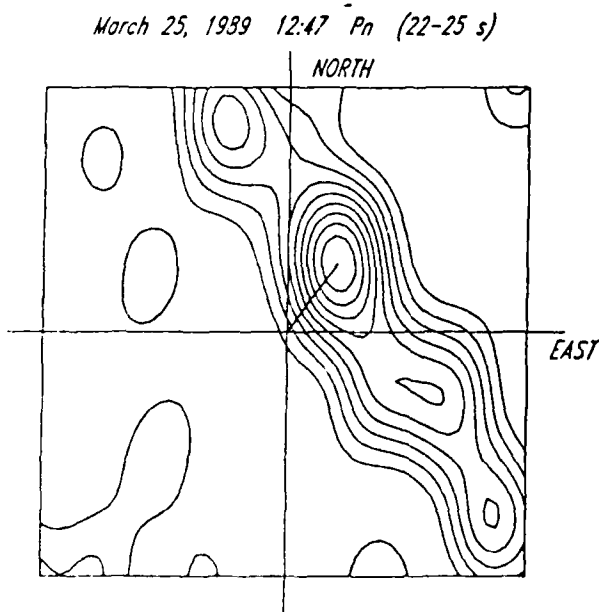
NBFK – single window

Estimated bearing: 36.984

Estimated velocity: 8.5702

Analysis frequency: 3.000

March 25, 1989 12:47 Pn (22-25 s)
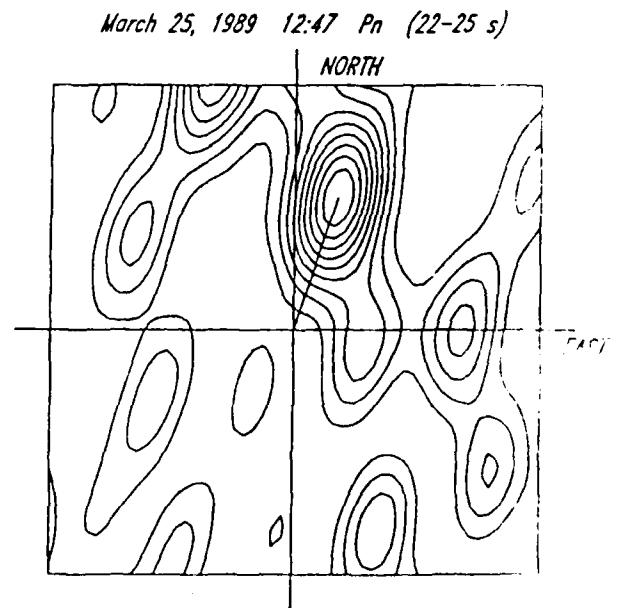
NBFK – single window

Estimated bearing: 17.627

Estimated velocity: 7.0533

Analysis frequency: 4.000

Fig. 33 :   Narrow-band wavenumber spectra of the Pn-phase of event no 1 from Table 1.
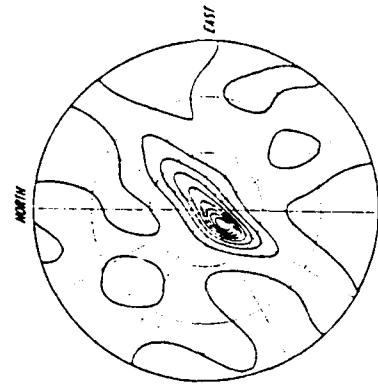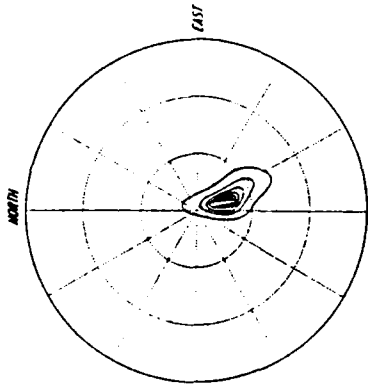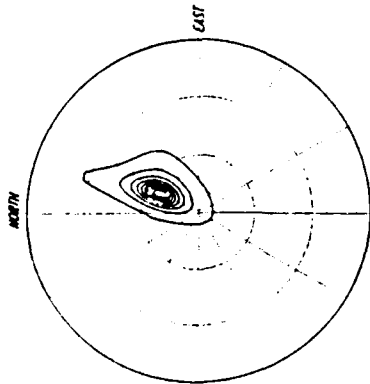
- 50 -
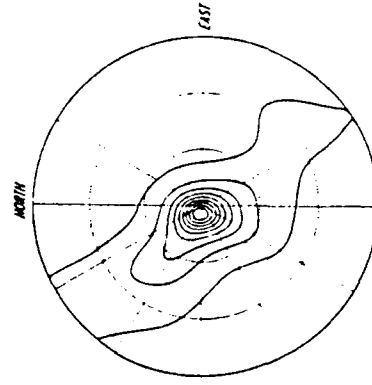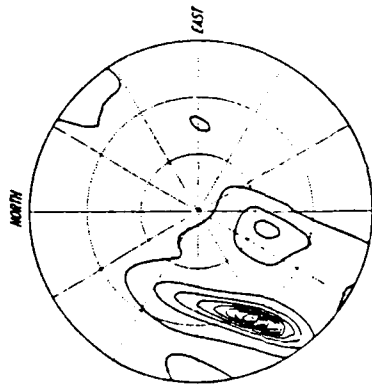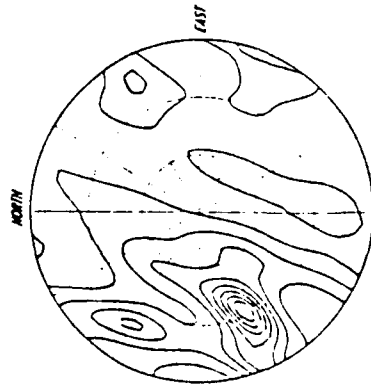
Fig. 34 :   Broad-band wavenumber spectra and azimuth estimates
of Pn-arrivals for 6 events from Table 1.

IV. Shallow Refraction Seismic Survey

A detailed geologic map of the array area is displayed in Figure 35. A comparison with topography shows that mainly the mountain tops consist of outcropping crystalline rock, i.e. granite and gneiss, whereas in the valleys a soil overburdens the basement rock. Due to this heterogeneity, the final siting of the array vaults was very difficult.

On the one hand the concentric ring geometry had to be born in mind, on the other hand as many seismometer sites as possible should be placed on bedrock.

An extensive refraction seismic survey was carried out to measure the depth of the bedrock. Altogether 43 reversed refraction profiles were shot which were distributed over the whole array area.

A twelve-channel Geometrics data acquisition system and a 12 kg hammer source was used. The spread of the in-line profiles varied between 24 m and 36 m (geophone distance of 2 m or 3 m respectively) with an offset of 2-3 m or 12-13 m. To increase the signal-to-noise ratio, 10-15 hammer blows were stacked.

The results of the survey are summarized in Table 2. The station names correspond to Figure 14. Often more than one profile had to be measured at each site and although the difference in location between profiles A,B or A,B,C was only of the order of 100 m, a large variation in interval velocities was found. This result reflects the complex surface geology of the area with varying overburden and weathering. In general the refraction survey yielded a three layer model: The first layer with interval velocities below 1000 m/s consists of soil, the second layer with interval velocities between 1000 m/s and 2000 m/s can be interpreted as more or less compact granitic or gneissic mud. Finally, the third layer with seismic velocities clearly above 2000 m/s represents weathered crystalline rock. In very few cases, crystalline bedrock with velocities above 4000 m/s was reached with the small-scale refraction method.

As a consequence of these results, it is not possible to place all seismometers of the 25-element array on bedrock, given a target depth of 4 - 5 m for the vaults. If the concentric-ring configuration is to be followed, the only alternative would be the installation of borehole seismometers. As no such instrumentation is planned for the GERESS array, it was made allowance of a deviation of the strict array geometry. By this procedure, most of the array sites are assumed to show noise values around 10 nm/s whereas a few mud sites may yield higher noise values up to 50 nm/s. Because these high values originate from a site amplification effect, also the seismic signals will be increased, and therefore the signal-to-noise ratio is comparable to the bedrock sites.

Array processing should take care of these different site characteristics and no major disadvantage in array performance is expected.

mica gneiss

andalusit gneiss

cordierite gneiss

coarse-grained Haidmühl granite

coarse-grained Haidmühl granite with cordierite gneiss fragments

medium-grained dike granite

diorite

fl   mud (fliesserde)

f   consolidated mud (fliesserde)

● GERESS array station
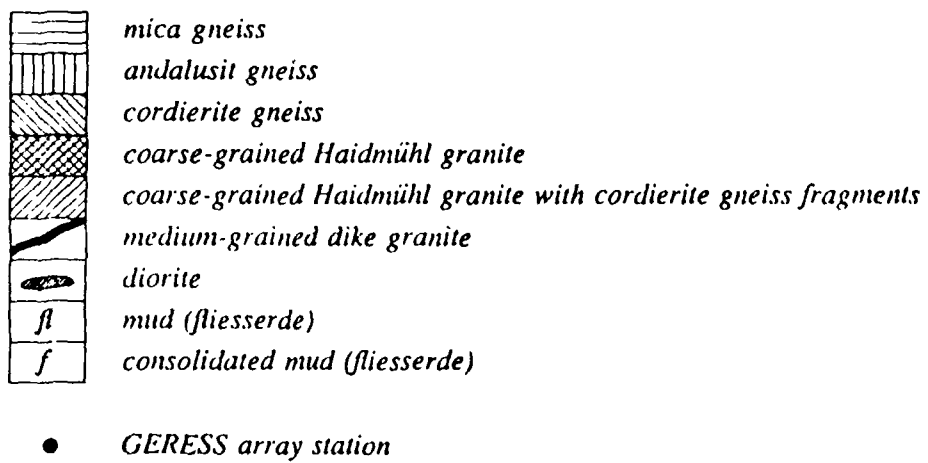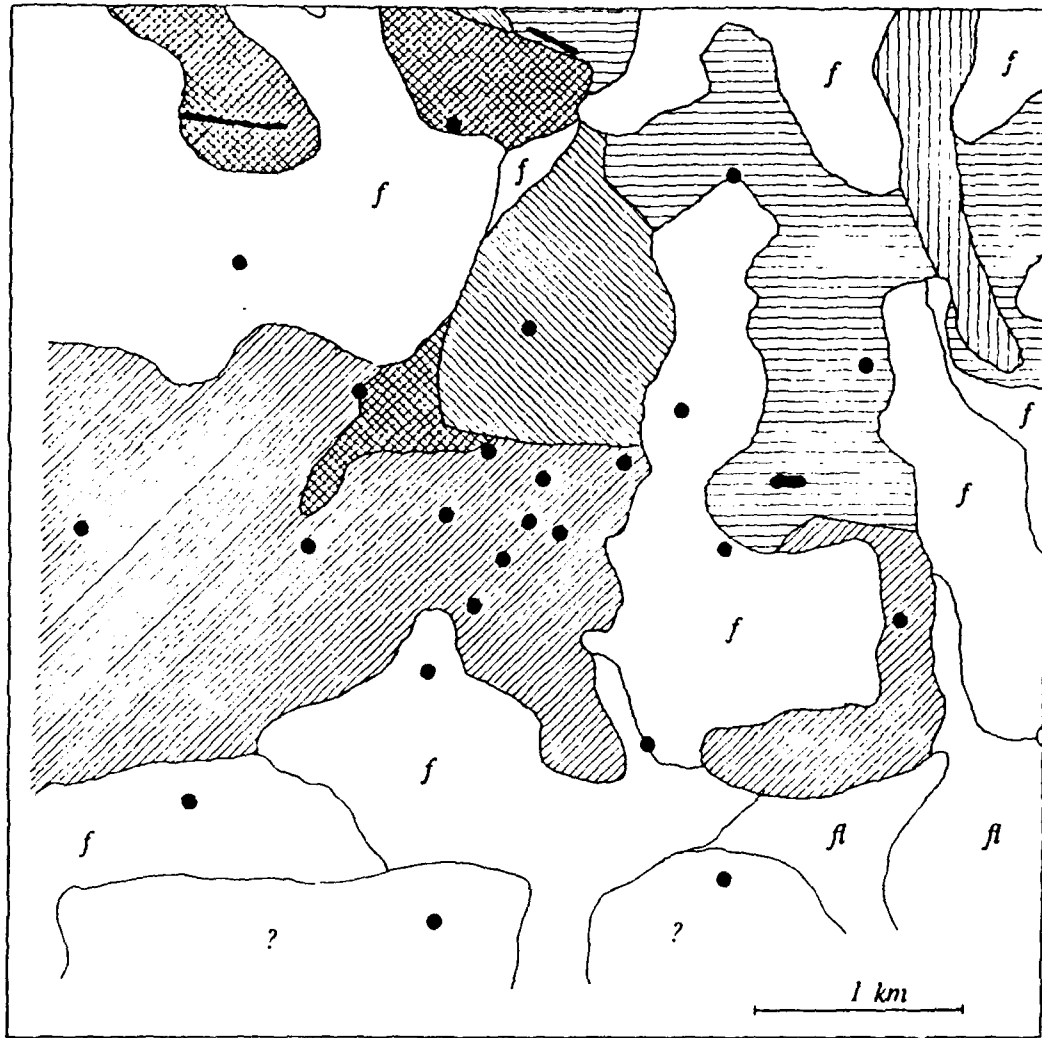
Fig. 35: Geological map of the GERESS array area

Table 2: Results of shallow refraction seismic survey

Station name	Interval velocities	Layer thicknesses upshooting	downshooting
Null A	v1= 330 m/s v2= 1550 m/s	3.2 m	3.1 m
Null B	v1= 360 m/s v2= 1200 m/s	4.5 m	1.7 m
Null C	v1= 370 m/s v2= 810 m/s	1.7 m	2.2 m
A3 A	v1= 380 m/s v2= 900 m/s v3= 2400 m/s	2.0 m 10.0 m	2.0 m 8.0 m
A3 B	v1= 400 m/s v2= 1050 m/s	3.0 m	1.3 m
B1	v1= 400 m/s v2= 900 m/s v3= 2800 m/s	1.0 m 12.0 m	3.0 m 7.4 m
B3	v1= 370 m/s v2= 640 m/s v3= 1900 m/s	2.3 m 9.3 m	3.0 m 7.5 m
B4 A	v1= 340 m/s v2= 950 m/s v3= 2000 m/s	1.4 m 10.0 m	2.2 m 9.3 m
B4 B	v1= 400 m/s v2= 800 m/s v3= 3100 m/s	1.6 m 4.0 m	0.5 m 11.0 m
B5 A	v1= 300 m/s v2= 850 m/s v3= 3000 m/s	1.0 m 4.0 m	
B5 B	v1= 410 m/s v2= 1000 m/s v3= 2200 m/s	1.5 m 4.0 m	1.5 m 4.4 m

C1 A	v1= 370 m/s	4.0 m	2.0 m
	v2= 1400 m/s	5.0 m	7.8 m
	v3= 2500 m/s		
C1 B	v1= 360 m/s	2.0 m	2.0 m
	v2= 830 m/s	7.0 m	5.6 m
	v3= 2800 m/s		
C1 C	v1= 350 m/s	2.0 m	3.3 m
	v2= 700 m/s		
C1 D	v1= 400 m/s	1.3 m	1.0 m
	v2= 800 m/s	6.4 m	6.0 m
	v3= 1900 m/s		
C3	v1= 360 m/s	2.7 m	
	v2= 1050 m/s	11.0 m	
	v3= 3300 m/s		
C4 A	v1= 600 m/s		2.5 m
	v2= 900 m/s		9.4 m
	v3= 4400 m/s		
C4 B	v1= 420 m/s	1.4 m	1.7 m
	v2= 670 m/s	7.0 m	1.9 m
	v3= 2050 m/s		
C4 C	v1= 730 m/s	5.5 m	6.8 m
	v2= 1900 m/s		
C5 A	v1= 370 m/s	3.4 m	2.3 m
	v2= 1400 m/s	9.0 m	7.0 m
	v3= 3400 m/s		
C5 B	v1= 330 m/s	0.5 m	1.3 m
	v2= 900 m/s	5.6 m	2.0 m
	v3= 1600 m/s		
C5 C	v1= 340 m/s	2.8 m	2.4 m
	v2= 2100 m/s		
C6 A	v1= 370 m/s	2.0 m	2.0 m
	v2= 2500 m/s		
C6 B	v1= 410 m/s	1.2 m	1.0 m
	v2= 1100 m/s	5.5 m	5.0 m
	v3= 2000 m/s		

C7	v1= 420 m/s	3.0 m	4.0 m
	v2= 2800 m/s	10.0 m	10.0 m
	v3= 5500 m/s		
D2 A	v1= 360 m/s	3.5 m	4.7 m
	v2= 1900 m/s		
D2 B	v1= 360 m/s	3.0 m	5.0 m
	v2= 2100 m/s		
D2 C	v1= 360 m/s	4.7 m	2.7 m
	v2= 2500 m/s		
D4 A	v1= 450 m/s	1.9 m	2.1 m
	v2= 1300 m/s	7.9 m	5.5 m
	v3= 4200 m/s		
D4 B	v1= 500 m/s	2.2 m	11.8 m
	v2= 1050 m/s	19.6 m	7.5 m
	v3= 4800 m/s		
D4 C	v1= 340 m/s	1.8 m	1.4 m
	v2= 1300 m/s		
D5 A	v1= 360 m/s	1.1 m	1.2 m
	v2= 1000 m/s	5.2 m	5.0 m
	v3= 1800 m/s		
D5 B	v1= 340 m/s	1.0 m	0.1 m
	v2= 900 m/s	2.5 m	1.6 m
	v3= 1400 m/s		
D5 C	v1= 370 m/s	1.4 m	1.0 m
	v2= 1030 m/s	5.6 m	3.0 m
	v3= 2200 m/s		
D6 A	v1= 520 m/s	10.1 m	2.7 m
	v2= 2200 m/s		
D6 B	v1= 390 m/s	1.0 m	0.3 m
	v2= 1320 m/s	15.0 m	9.3 m
	v3= 5600 m/s		
D7 A	v1= 350 m/s	1.5 m	
	v2= 600 m/s	4.0 m	
	v3= 4000 m/s		

D7 B	v1= 370 m/s	1.3 m	1.5 m
	v2= 1600 m/s	6.3 m	9.4 m
	v3= 3700 m/s		
D8 A	v1= 660 m/s	5.0 m	5.0 m
	v2= 1700 m/s		
D8 B	v1= 530 m/s	4.0 m	2.0 m
	v2= 1050 m/s	11.0 m	10.0 m
	v3= 2800 m/s		
D9 A	v1= 340 m/s	0.7 m	1.2 m
	v2= 700 m/s	16.0 m	13.0 m
	v3= 3400 m/s		
D9 B	v1= 340 m/s	4.3 m	5.5 m
	v2= 2200 m/s		
D9 C	v1= 350 m/s	1.6 m	3.8 m
	v2= 800 m/s		

V. Acknowledgements

Prof. Thomas Ahrens
Seismological Lab, 252-21
Division of Geological & Planetary Sciences
California Institute of Technology
Pasadena, CA 91125

Prof. Charles B. Archambeau
CIRES
University of Colorado
Boulder, CO 80309

Dr. Thomas C. Bache, Jr.
Science Applications Int'l Corp.
10260 Campus Point Drive
San Diego, CA 92121   (2 copies)

Prof. Muawia Barazangi
Institute for the Study of the Continent
Cornell University
Ithaca, NY 14853

Dr. Douglas R. Baumgardt
ENSCO, Inc
5400 Port Royal Road
Springfield, VA 22151-2388

Prof. Jonathan Berger
IGPP, A-025
Scripps Institution of Oceanography
University of California, San Diego
La Jolla, CA 92093

Dr. Lawrence J. Burdick
Woodward-Clyde Consultants
566 El Dorado Street
Pasadena, CA 91109-3245

Dr. Karl Coyner
New England Research, Inc.
76 Olcott Drive
White River Junction, VT 05001

Prof. Vernon F. Cormier
Department of Geology & Geophysics
U-45, Room 207
The University of Connecticut
Storrs, CT 06268

Professor Anton W. Dainty
Earth Resources Laboratory
Massachusetts Institute of Technology
42 Carleton Street
Cambridge, MA 02142

Prof. Steven Day
Department of Geological Sciences
San Diego State University
San Diego, CA 92182

Dr. Zoltan A. Der
ENSCO, Inc.
5400 Port Royal Road
Springfield, VA 22151-2388

Prof. John Ferguson
Center for Lithospheric Studies
The University of Texas at Dallas
P.O. Box 830688
Richardson, TX 75083-0688

Prof. Stanley Flatte
Applied Sciences Building
University of California
Santa Cruz, CA 95064

Dr. Alexander Florence
SRI International
333 Ravenswood Avenue
Menlo Park, CA 94025-3493

Prof. Henry L. Gray
Vice Provost and Dean
Department of Statistical Sciences
Southern Methodist University
Dallas, TX 75275

Dr. Indra Gupta
Teledyne Geotech
314 Montgomery Street
Alexandria, VA 22314

Prof. David G. Harkrider
Seismological Laboratory
Division of Geological & Planetary Sciences
California Institute of Technology
Pasadena, CA 91125

Prof. Donald V. Helmberger
Seismological Laboratory
Division of Geological & Planetary Sciences
California Institute of Technology
Pasadena, CA 91125

Prof. Eugene Herrin
Institute for the Study of Earth and Man
GeophysicalLaboratory
Southern Methodist University
Dallas, TX 75275

Prof . Robert B. Herrmann
Department of Earth & Atmospheric Sciences
St. Louis University
St. Louis, MO 63156

Dr. Christopher Lynnes
Teledyne Geotech
314 Montgomery Street
Alexandria, VA 22314

Prof. Bryan Isacks
Cornell University
Department of Geological Sciences
SNEE Hall
Ithaca, NY 14850

Prof. Peter Malin
University of California at Santa Barbara
Institute for Crustal Studies
Santa Barbara, CA 93106

Dr. Rong-Song Jih
Teledyne Geotech
314 Montgomery Street
Alexandria, VA 22314

Dr. Randolph Martin, III
New England Research, Inc.
76 Olcott Drive
White River Junction, VT 05001

Prof. Lane R. Johnson
Seismographic Station
University of California
Berkeley, CA 94720

Dr. Gary McCartor
Mission Research Corporation
735 State Street
P.O. Drawer 719
Santa Barbara, CA 93102 (2 copies)

Prof. Alan Kafka
Department of Geology & Geophysics
Boston College
Chestnut Hill, MA 02167

Prof. Thomas V. McEvilly
Seismographic Station
University of California
Berkeley, CA 94720

Dr. Richard LaCoss
MIT-Lincoln Laboratory
M-200B
P. O. Box 73
Lexington, MA 02173-0073 (3 copies)

Dr. Keith L. McLaughlin
S-CUBED
A Division of Maxwell Laboratory
P.O. Box 1620
La Jolla, CA 92038-1620

Prof Fred K. Lamb
University of Illinois at Urbana-Champaign
Department of Physics
1110 West Green Street
Urbana, IL 61801

Prof. William Menke
Lamont-Doherty Geological Observatory
of Columbia University
Palisades, NY 10964

Prof. Charles A. Langston
Geosciences Department
403 Deike Building
The Pennsylvania State University
University Park, PA 16802

Stephen Miller
SRI International
333 Ravenswood Avenue
Box AF 116
Menlo Park, CA 94025-3493

Prof. Thorne Lay
Institute of Tectonics
Earth Science Board
University of California, Santa Cruz
Santa Cruz, CA 95064

Prof. Bernard Minster
IGPP, A-025
Scripps Institute of Oceanography
University of California, San Diego
La Jolla, CA 92093

Prof. Arthur Lerner-Lam
Lamont-Doherty Geological Observatory
of Columbia University
Palisades, NY 10964

Prof. Brian J. Mitchell
Department of Earth & Atmospheric Sciences
St. Louis University
St. Louis, MO 63156

Mr. Jack Murphy
S-CUBED, A Division of Maxwell Laboratory
11800 Sunrise Valley Drive
Suite 1212
Reston, VA 22091 (2 copies)

Dr. Bao Nguyen
GL/LWH
Hanscom AFB, MA 01731-5000

Prof. John A. Orcutt
IGPP, A-025
Scripps Institute of Oceanography
University of California, San Diego
La Jolla, CA 92093

Prof. Keith Priestley
University of Cambridge
Bullard Labs, Dept. of Earth Sciences
Madingley Rise, Madingley Rd.
Cambridge CB3 OEZ, ENGLAND

Prof. Paul G. Richards
L-210
Lawrence Livermore National Laboratory
Livermore, CA 94550

Dr. Wilmer Rivers
Teledyne Geotech
314 Montgomery Street
Alexandria, VA 22314

Prof. Charles G. Sammis
Center for Earth Sciences
University of Southern California
University Park
Los Angeles, CA 90089-0741

Prof. Christopher H. Scholz
Lamont-Doherty Geological Observatory
of Columbia University
Palisades, NY 10964

Thomas J. Sereno, Jr.
Science Application Int'l Corp.
10260 Campus Point Drive
San Diego, CA 92121

Prof. David G. Simpson
Lamont-Doherty Geological Observatory
of Columbia University
Palisades, NY 10964

Dr. Jeffrey Stevens
S-CUBED
A Division of Maxwell Laboratory
P.O. Box 1620
La Jolla, CA 92038-1620

Prof. Brian Stump
Institute for the Study of Earth & Man
Geophysical Laboratory
Southern Methodist University
Dallas, TX 75275

Prof. Jeremiah Sullivan
University of Illinois at Urbana-Champaign
Department of Physics
1110 West Green Street
Urbana, IL 61801

Prof. Clifford Thurber
University of Wisconsin-Madison
Department of Geology & Geophysics
1215 West Dayton Street
Madison, WS 53706

Prof. M. Nafi Toksoz
Earth Resources Lab
Massachusetts Institute of Technology
42 Carleton Street
Cambridge, MA 02142

Prof. John E. Vidale
University of California at Santa Cruz
Seismological Laboratory
Santa Cruz, CA 95064

Prof. Terry C. Wallace
Department of Geosciences
Building #77
University of Arizona
Tucson, AZ 85721

Dr. Raymond Willeman
GL/LWH
Hanscom AFB, MA 01731-5000

Dr. Lorraine Wolf
GL/LWH
Hanscom AFB, MA 01731-5000

Dr. Monem Abdel-Gawad
Rockwell International Science Center
1049 Camino Dos Rios
Thousand Oaks, CA 91360

Prof. Keiiti Aki
Center for Earth Sciences
University of Southern California
University Park
Los Angeles, CA 90089-0741

Prof. Shelton S. Alexander
Geosciences Department
403 Deike Building
The Pennsylvania State University
University Park, PA 16802

Dr. Kenneth Anderson
BBNSTC
Mail Stop 14/1B
Cambridge, MA 02238

Dr. Ralph Archuleta
Department of Geological Sciences
University of California at Santa Barbara
Santa Barbara, CA 93102

J. Barker
Department of Geological Sciences
State University of New York
at Binghamton
Vestal, NY 13901

Dr. T.J. Bennett
S-CUBED
A Division of Maxwell Laboratory
11800 Sunrise Valley Drive, Suite 1212
Reston, VA 22091

Mr. William J. Best
907 Westwood Drive
Vienna, VA 22180

Dr. N. Biswas
Geophysical Institute
University of Alaska
Fairbanks, AK 99701

Dr. G.A. Bollinger
Department of Geological Sciences
Virginia Polytechnical Institute
21044 Derring Hall
Blacksburg, VA 24061

Dr. Stephen Bratt
Center for Seismic Studies
1300 North 17th Street
Suite 1450
Arlington, VA 22209

Michael Browne
Teledyne Geotech
3401 Shiloh Road
Garland, TX 75041

Mr. Roy Burger
1221 Serry Road
Schenectady, NY 12309

Dr. Robert Burridge
Schlumberger-Doll Research Center
Old Quarry Road
Ridgefield, CT 06877

Dr. Jerry Carter
Rondout Associates
P.O. Box 224
Stone Ridge, NY 12484

Dr. W. Winston Chan
Teledyne Geotech
314 Montgomery Street
Alexandria, VA 22314-1581

Dr. Theodore Cherry
Science Horizons, Inc.
710 Encinitas Blvd., Suite 200
Encinitas, CA 92024 (2 copies)

Prof. Jon F. Claerbout
Department of Geophysics
Stanford University
Stanford, CA 94305

Prof. Robert W. Clayton
Seismological Laboratory
Division of Geological & Planetary Sciences
California Institute of Technology
Pasadena, CA 91125

Prof. F. A. Dahlen
Geological and Geophysical Sciences
Princeton University
Princeton, NJ 08544-0636

Prof. Adam Dziewonski
Hoffman Laboratory
Harvard University
20 Oxford St
Cambridge, MA 02138

Prof. John Ebel
Department of Geology & Geophysics
Boston College
Chestnut Hill, MA 02167

Eric Fielding
SNEE Hall
INSTOC
Cornell University
Ithaca, NY 14853

Prof. Donald Forsyth
Department of Geological Sciences
Brown University
Providence, RI 02912

Dr. Cliff Frolich
Institute of Geophysics
8701 North Mopac
Austin, TX 78759

Prof. Art Frankel
Mail Stop 922
Geological Survey
790 National Center
Reston, VA 22092

Dr. Anthony Gangi
Texas A&M University
Department of Geophysics
College Station, TX 77843

Dr Freeman Gilbert
Inst. of Geophysics & Planetary Physics
University of California, San Diego
P.O. Box 109
La Jolla, CA 92037

Mr. Edward Giller
Pacific Sierra Research Corp.
1401 Wilson Boulevard
Arlington, VA 22209

Dr. Jeffrey W. Given
Sierra Geophysics
11255 Kirkland Way
Kirkland, WA 98033

Prof. Stephen Grand
University of Texas at Austin
Department of Geological Sciences
Austin, TX 78713-7909

Prof. Roy Greenfield
Geosciences Department
403 Deike Building
The Pennsylvania State University
University Park, PA 16802

Dan N. Hagedorn
Battelle
Pacific Northwest Laboratories
Battelle Boulevard
Richland, WA 99352

Kevin Hutchenson
Department of Earth Sciences
St. Louis University
3507 Laclede
St. Louis, MO 63103

Prof. Thomas H. Jordan
Department of Earth, Atmospheric
  and Planetary Sciences
Massachusetts Institute of Technology
Cambridge, MA 02139

Robert C. Kemerait
ENSCO, Inc.
445 Pineda Court
Melbourne, FL 32940

William Kikendall
Teledyne Geotech
3401 Shiloh Road
Garland, TX 75041

Prof. Leon Knopoff
University of California
Institute of Geophysics & Planetary Physics
Los Angeles, CA 90024

Prof. L. Timothy Long
School of Geophysical Sciences
Georgia Institute of Technology
Atlanta, GA 30332

Prof. Art McGarr
Mail Stop 977
Geological Survey
345 Middlefield Rd.
Menlo Park, CA 94025

Dr. George Mellman
Sierra Geophysics
11255 Kirkland Way
Kirkland, WA 98033

Dr. Richard Sailor
TASC Inc.
55 Walkers Brook Drive
Reading, MA 01867

Prof. John Nabelek
College of Oceanography
Oregon State University
Corvallis, OR 97331

John Sherwin
Teledyne Geotech
3401 Shiloh Road
Garland, TX 75041

Prof. Geza Nagy
University of California, San Diego
Department of Ames, M.S. B-010
La Jolla, CA 92093

Prof. Robert Smith
Department of Geophysics
University of Utah
1400 East 2nd South
Salt Lake City, UT 84112

Prof. Amos Nur
Department of Geophysics
Stanford University
Stanford, CA 94305

Prof. S. W. Smith
Geophysics Program
University of Washington
Seattle, WA 98195

Prof. Jack Oliver
Department of Geology
Cornell University
Ithaca, NY 14850

Dr. Stewart Smith
IRIS Inc.
1616 North Fort Myer Drive
Suite 1440
Arlington, VA 22209

Prof. Robert Phinney
Geological & Geophysical Sciences
Princeton University
Princeton, NJ 08544-0636

Dr. George Sutton
Rondout Associates
P.O. Box 224
Stone Ridge, NY 12484

Dr. Paul Pomeroy
Rondout Associates
P.O. Box 224
Stone Ridge, NY 12484

Prof. L. Sykes
Lamont-Doherty Geological Observatory
of Columbia University
Palisades, NY 10964

Dr. Jay Pulli
RADIX System, Inc.
2 Taft Court, Suite 203
Rockville, MD 20850

Prof. Pradeep Talwani
Department of Geological Sciences
University of South Carolina
Columbia, SC 29208

Dr. Norton Rimer
S CUBED
A Division of Maxwell Laboratory
P.O. Box 1620
La Jolla, CA 92038-1620

Prof. Ta-liang Teng
Center for Earth Sciences
University of Southern California
University Park
Los Angeles, CA 90089-0741

Prof. Larry J. Ruff
Department of Geological Sciences
1006 C.C. Little Building
University of Michigan
Ann Arbor, MI 48109-1063

Dr. R.B. Tittmann
Rockwell International Science Center
1049 Camino Dos Rios
P.O. Box 1085
Thousand Oaks, CA 91360

Dr. Gregory van der Vink
IRIS, Inc.
1616 North Fort Myer Drive
Suite 1440
Arlington, VA 22209

Professor Daniel Walker
University of Hawaii
Institute of Geophysics
Honolulu, HI 96822

William R. Walter
Seismological Laboratory
University of Nevada
Reno, NV 89557

Dr. Gregory Wojcik
Weidlinger Associates
4410 El Camino Real
Suite 110
Los Altos, CA 94022

Prof. John H. Woodhouse
Hoffman Laboratory
Harvard University
20 Oxford St.
Cambridge, MA 02138

Prof. Francis T. Wu
Department of Geological Sciences
State University of New York
at Binghamton
Vestal, NY 13901

Dr. Gregory B. Young
ENSCO, Inc.
5400 Port Royal Road
Springfield, VA 22151-2388

Dr. Ralph Alewine III
DARPA/NMRO
1400 Wilson Boulevard
Arlington, VA 22209-2308

Paul Johnson
ESS-4, Mail Stop J979
Los Alamos National Laboratory
Los Alamos, NM 87545

Mr. James C. Battis
GL/LWH
Hanscom AFB, MA 01731-5000

Janet Johnston
GL/LWH
Hanscom AFB, MA 01731-5000

Dr. Robert Blandford
DARPA/NMRO
1400 Wilson Boulevard
Arlington, VA 22209-2308

Dr. Katharine Kadinsky-Cade
GL/LWH
Hanscom AFB, MA 01731-5000

Eric Chael
Division 9241
Sandia Laboratory
Albuquerque, NM 87185

Ms. Ann Kerr
IGPP, A-025
Scripps Institute of Oceanography
University of California, San Diego
La Jolla, CA 92093

Dr. John J. Cipar
GL/LWH
Hanscom AFB, MA 01731-5000

Dr. Max Koontz
US Dept of Energy/DP 5
Forrestal Building
1000 Independence Avenue
Washington, DC 20585

Mr. Jeff Duncan
Office of Congressman Markey
2133 Rayburn House Bldg.
Washington, DC 20515

Dr. W.H.K. Lee
Office of Earthquakes, Volcanoes,
& Engineering
345 Middlefield Road
Menlo Park, CA 94025

Dr. Jack Evernden
USGS - Earthquake Studies
345 Middlefield Road
Menlo Park, CA 94025

Dr. William Leith
U.S. Geological Survey
Mail Stop 928
Reston, VA 22092

Art Frankel
USGS
922 National Center
Reston, VA 22092

Dr. Richard Lewis
Director, Earthquake Engineering & Geophysics
U.S. Army Corps of Engineers
Box 631
Vicksburg, MS 39180

Dr. T. Hanks
USGS
Nat'l Earthquake Research Center
345 Middlefield Road
Menlo Park, CA 94025

James F. Lewkowicz
GL/LWH
Hanscom AFB, MA 01731-5000

Dr. James Hannon
Lawrence Livermore Nat'l Laboratory
P.O. Box 808
Livermore, CA 94550

Mr. Alfred Lieberman
ACDA/VI-OA'State Department Bldg
Room 5726
320 - 21st Street, NW
Washington, DC 20451

Stephen Mangino
GL/LWH
Hanscom AFB, MA 01731-5000

Dr. Frank F. Pilotte
HQ AFTAC/TT
Patrick AFB, FL 32925-6001

Dr. Robert Masse
Box 25046, Mail Stop 967
Denver Federal Center
Denver, CO 80225

Katie Poley
CIA-OSWR/NED
Washington, DC 20505

Art McGarr
U.S. Geological Survey, MS-977
345 Middlefield Road
Menlo Park, CA 94025

Mr. Jack Rachlin
U.S. Geological Survey
Geology, Rm 3 C136
Mail Stop 928 National Center
Reston, VA 22092

Richard Morrow
ACDA/VI, Room 5741
320 21st Street N.W
Washington, DC 20451

Dr. Robert Reinke
WL/NTESG
Kirtland AFB, NM 87117-6008

Dr. Keith K. Nakanishi
Lawrence Livermore National Laboratory
P.O. Box 808, L-205
Livermore, CA 94550

Dr. Byron Ristvet
HQ DNA, Nevada Operations Office
Attn: NVCG
P.O. Box 98539
Las Vegas, NV 89193

Dr. Carl Newton
Los Alamos National Laboratory
P.O. Box 1663
Mail Stop C335, Group ESS-3
Los Alamos, NM 87545

Dr. George Rothe
HQ AFTAC/TGR
Patrick AFB, FL 32925-6001

Dr. Kenneth H. Olsen
Los Alamos Scientific Laboratory
P.O. Box 1663
Mail Stop C335, Group ESS-3
Los Alamos, NM 87545

Dr. Alan S. Ryall, Jr.
DARPA/NMRO
1400 Wilson Boulevard
Arlington, VA 22209-2308

Howard J. Patton
Lawrence Livermore National Laboratory
P.O. Box 808, L-205
Livermore, CA 94550

Dr. Michael Shore
Defense Nuclear Agency/SPSS
6801 Telegraph Road
Alexandria, VA 22310

Mr. Chris Paine
Office of Senator Kennedy
SR 315
United States Senate
Washington, DC 20510

Dr. Albert Smith
Los Alamos National Laboratory
L-205
P. O. Box 808
Livermore, CA 94550

Colonel Jerry J. Perrizo
AFOSR/NP, Building 410
Bolling AFB
Washington, DC 20332-6448

Donald L. Springer
Lawrence Livermore National Laboratory
L-205
P. O. Box 808
Livermore , CA 94550

Mr. Charles L. Taylor
GL/LWG
Hanscom AFB, MA 01731-5000

DARPA/RMO/Security Office
1400 Wilson Boulevard
Arlington, VA 22209

Mr. Steven R. Taylor
Lawrence Livermore National Laboratory
L-205
P. O. Box 808
Livermore, CA 94550

Geophysics Laboratory
Attn: XO
Hanscom AFB, MA 01731-5000

Dr. Eileen Vergino
Lawrence Livermore National Laboratory
L-205
P. O. Box 808
Livermore, CA 94550

Geophysics Laboratory
Attn: LW
Hanscom AFB, MA 01731-5000

Dr. Thomas Weaver
Los Alamos National Laboratory
P.O. Box 1663, Mail Stop C335
Los Alamos, NM 87545

DARPA/PM
1400 Wilson Boulevard
Arlington, VA 22209

J.J. Zucca
Lawrence Livermore National Laboratory
P. O. Box 808
Livermore, CA 94550

Defense Technical Information Center
Cameron Station
Alexandria, VA 22314 (5 copies)

GL/SULL
Research Library
Hanscom AFB , MA 01731-5000 (2 copies)

Defense Intelligence Agency
Directorate for Scientific
& Technical IntelligenceAttn: DT1B
Washington, DC 20340-6158

Secretary of the Air Force
(SAFRD)
Washington, DC 20330

AFTAC/CA
(STINFO)
Patrick AFB, FL 32925-6001

Office of the Secretary Defense
DDR & E
Washington, DC 20330

TACTEC
Battelle Memorial Institute
505 King Avenue
Columbus, OH 43201 (Final Report Only)

HQ DNA
Attn: Technical Library
Washington, DC 20305

DARPA/RMO/RETRIEVAL
1400 Wilson Boulevard
Arlington, VA 22209

Dr. Ramon Cabre, S.J.
Observatorio San Calixto
Casilla 5939
La Paz, Bolivia

Prof. Hans-Peter Harjes
Institute for Geophysik
Ruhr University/Bochum
P.O. Box 102148
4630 Bochum 1, FRG

Prof. Eystein Husebye
NTNF/NORSAR
P.O. Box 51
N-2007 Kjeller, NORWAY

Prof. Brian L.N. Kennett
Research School of Earth Sciences
Institute of Advanced Studies
G.P.O. Box 4
Canberra 2601, AUSTRALIA

Dr. Bernard Massinon
Societe Radiomana
27 rue Claude Bernard
75005 Paris, FRANCE (2 Copies)

Dr. Pierre Mecheler
Societe Radiomana
27 rue Claude Bernard
75005 Paris, FRANCE

Dr. Svein Mykkeltveit
NTNF/NORSAR
P.O. Box 51
N-2007 Kjeller, NORWAY

Dr. Peter Basham
Earth Physics Branch
Geological Survey of Canada
1 Observatory Crescent
Ottawa, Ontario, CANADA K1A 0Y3

Dr. Eduard Berg
Institute of Geophysics
University of Hawaii
Honolulu, HI 96822

Dr. Michel Bouchon
I.R.I.G.M.-B.P. 68
38402 St. Martin D'Heres
Cedex, FRANCE

Dr. Hilmar Bungum
NTNF/NORSAR
P.O. Box 51
N-2007 Kjeller, NORWAY

Dr. Michel Campillo
Observatoire de Grenoble
I.R.I.G.M.-B.P. 53
38041 Grenoble, FRANCE

Dr. Kin Yip Chun
Geophysics Division
Physics Department
University of Toronto
Ontario, CANADA M5S 1A7

Dr. Alan Douglas
Ministry of Defense
Blacknest, Brimpton
Reading RG7-4RS, UNITED KINGDOM

Dr. Roger Hansen
NTNF/NORSAR
P.O. Box 51
N-2007 Kjeller, NORWAY

Dr. Manfred Henger
Federal Institute for Geosciences & Nat'l Res.
Postfach 510153
D-3000 Hanover 51, FRG

Ms. Eva Johannisson
Senior Research Officer
National Defense Research Inst.
P.O. Box 27322
S-102 54 Stockholm, SWEDEN

Dr. Fekadu Kebede
Seismological Section
Box 12019
S-750 Uppsala, SWEDEN

Dr. Tormod Kvaerna
NTNF/NORSAR
P.O. Box 51
N-2007 Kjeller, NORWAY

Dr. Peter Marshal
Procurement Executive
Ministry of Defense
Blacknest, Brimpton
Reading FG7-4RS, UNITED KINGDOM

Prof. Ari Ben-Menahem
Department of Applied Mathematics
Weizman Institute of Science
Rehovot, ISRAEL 951729

Dr. Robert North
Geophysics Division
Geological Survey of Canada
1 Observatory Crescent
Ottawa, Ontario, CANADA K1A 0Y3

Dr. Frode Ringdal
NTNF/NORSAR
P.O. Box 51
N-2007 Kjeller, NORWAY

Dr. Jorg Schlittenhardt
Federal Institute for Geosciences & Nat'l Res.
Postfach 510153
D-3000 Hannover 51, FEDERAL REPUBLIC OF
GERMANY